Construction and Building Materials 347 (2022) 128548

Contents lists available at ScienceDirect

Construction and Building Materials

journal homepage: www.elsevier.com/locate/conbuildmat

Investigation of mechanical and durability properties of brick powder-added White Cement composites with three different fibers

Mahmood Anwar Shaker Alcharchafche [a], Mukhallad M. Al-mashhadani [a,*], Yurdakul Aygörmez [b]

[a] Istanbul Gelisim University, Civil Engineering Department, Avcilar Campus, Istanbul, Turkey
[b] Yildiz Technical University, Civil Engineering Department, Davutpasa Campus, Istanbul, Turkey

ARTICLE INFO

Keywords:
White Cement
Brick powder
Crimped steel fiber
Copper-coated steel fiber
Basalt fiber
High-temperature test
Freezing-thawing test
Sulfate attack test

ABSTRACT

Traditional Portland Cement is used extensively in the construction industry today. Portland Cement has a gray color and has been explored with numerous substitutes. With the increasing interest in concrete technology, the interest in composite materials with higher performance and strength has gained more importance. White Cement (WC) is an important cement type in this field. However, studies of substitute materials for White Cement are limited and more research is needed. In this study, while White Cement and clay brick powder (CBP) were substituted at three different rates (5%, 10%, and 15%), three different fibers (copper-coated (CC) steel fiber, crimped (C) steel fiber, and basalt (B) fiber) were used at the ratio of 0.4% to examine the effect of fibers at the same time. The compressive and flexural strengths of the prepared series were investigated for 28 and 90 days. Three different durability tests were applied after 90 days: elevated-temperature test (250, 500, and 750 °C), freezing-thawing test (90 cycles), and sulfate effect (90 days). Following the durability tests, weight and strength values were compared. In addition, SEM and XRD analyzes were made while making comparisons before and after the durability test of the samples and a visual examination was made in the durability conditions. The use of 5% brick powder increased the strength values due to the formation of C-A-S-H and C-S-H gels due to its higher Al_2O_3 and SiO_2 content, while the use of higher brick powder caused a decrease in strength. While the fibers contributed positively to the strength values, the highest increase was in the longer crimped steel fiber added sample and the lowest increase was in the shorter copper-coated steel fiber added sample. While there was a 13% increase in compressive strength in the crimped steel fiber and 5% brick dust added sample compared to the control sample, there was a 21% increase in flexural strength. As a result of the durability tests, the samples behaved in similar order and maintained their stability despite significant losses.

1. Introduction

Cementitious materials hold inevitable importance among the various materials used in construction applications. Economical and structural advantages are the main reasons that contribute to making cement-based composites extensive, constructors always tend to conduct structural works with materials that are comparable in all aspects. In addition to that, cement-based composites are sufficiently detailed in the local and international standards worldwide, which makes them preferable in design procedures.

However, the production process of cement causes different environmental problems, it starts with consuming natural resources and energy and ends with carbon dioxide emissions which are considered one of the major reasons for pollution. In this field, the worldwide statistics proved the fact that the cement industry is causing at least 7–8% of the total CO_2 emissions around the globe. Not to mention the other emissions that accompany the process of cement production like carbon monoxide and other greenhouse gases [1–4].

Also, composites that are manufactured based on cementitious materials are prone to different physical, chemical, and structural drawbacks. Critical factors in this process (cement type, mix proportions, the existence of admixtures, curing details…. etc.) play an important role in determining the properties of the resulting composite such as strength, durability, and long-term properties [5,6].

The aforementioned disadvantages are the main motivating factor for many researchers to enhance the final cementitious product, various

* Corresponding author.
E-mail address: mashhadani@gelisim.edu.tr (M.M. Al-mashhadani).

https://doi.org/10.1016/j.conbuildmat.2022.128548
Received 30 January 2022; Received in revised form 16 July 2022; Accepted 19 July 2022
Available online 28 July 2022

experimental attempts were conducted in this concern to minimize the environmental footprint or to improve the properties of the fabricated material. Partial or full replacement of cement with other materials such as waste materials or naturally available unused materials represented the core of the research performed in this field [7–9].

Although some research ideas were also based on using other types of cement, they were beneficial in illustrating the main concept of comparison between various types of cement. For instance, Ginting et al. [10] conducted an experimental investigation to compare gray and White Cement concerning their fresh and hardened properties. The conclusions revealed the fact that fabricating White Cement composites yielded relatively weaker performance in the fresh state but a significant improvement in terms of compressive and tensile strengths. This is related to the fact that silicate percentages were relatively higher in White Cement which contributes to enhancing the ultimate strength of the fabricated specimens.

Yang et al. [11] investigated the effect of combined wetting–drying cycles along with external sulfate attack on white cement-based mortars by conducting some microstructural analyses. The main findings of the research stated the fact that Ettringite is the principal cause for deteriorations that are caused by the aforementioned exposure types.

Zhang et al. [12] researched to examine the effect of incorporating different Nanoparticles on the hydration mechanism and strength properties of white cement-based mortar. The main conclusions of this work revealed the fact that Nanoparticles helped to decrease the initial and final setting times of the matrix, also, the strength of the fabricated specimens was improved because of the achieved compactness as well as the good degree of bonding between the matrix and the used Nanoparticles.

Some research topics were aiming to enhance the performance of the cementitious matrix by using blended cement types of cement of using special types of cement which are designated for different aspects. Joshaghani [13] conducted experimental research to highlight the importance of using titanium nanoparticles as a replacement for limestone cement mortar. The findings of the research showed that the existence of these particles helped in improving the microstructure of the cementitious matrix as well as the resistance to chloride penetration.

On the other hand, using materials such as ceramic waste or brick waste as a partial replacement within the cementitious matrix. This approach is advantageous in terms of sustainability and utilizing waste. Furthermore, using such materials might be a reason for improving the properties of the resulting material in terms of strength and performance against various conditions.

Within this scope, many research attempts were carried out to investigate the effect of using the aforementioned materials. Huang et al. [14] tested the effect of using waste clay brick on the mechanical properties and water absorption of the fabricated mortar specimens, the results showed that using the aforementioned waste material helped in improving mechanical properties as well as the bonding degree and the rate of hydration for the resulting binding materials.

Lam [15] investigated the feasibility of using clay powder waste on the heat performance of the fabricated composites that contained this waste along with Portland cement, the main findings of the research stated that the replacement used yielded adequate performance in terms of heat resistance in 800 °C and 1000 °C. Also, the using clay brick powder resulted in creating a sintering effect in the fabricated matrix which helped in enhancing the thermal stability of the mortars.

Also, Shao et al. [16] performed a study to illustrate the pozzolanic behavior of cement-clay brick powder blended pastes, their study was based on the concept of increasing the level of replacement with cement, and the general conclusion that further replacement levels are shown to decrease the strength performance of the specimens. However, their results stated that the pozzolanic reaction of clay brick powder was found to enhance the strength of the pastes up to a certain limit of replacement.

On the other hand, many research attempts focused on enhancing the brittle behavior of the conventional cementitious matrix by using fibers to get good results in terms of flexural performance. In this field, some investigations were made on both traditional Portland Cement and White Cement, Zhang et al. [17] tested the effect of using both recycled brick powder waste and polypropylene fibers on the workability and mechanical properties of Portland cement-based composites and they concluded that using the aforementioned materials can result in decreasing workability because of high water absorption rate of PP fibers. On the other hand, their findings showed that strength properties such as compressive and tensile strength showed an improvement when clay brick powder and fibers were used.

Dilbas and Çakır [18] investigated the effect of using basalt fiber along with recycled aggregates on the physical and mechanical properties of concrete. According to their results, the existence of both recycled aggregates and basalt fibers resulted in a negative effect concerning physical properties. However, using basalt fibers was found to be beneficial in terms of improving the compressive strength of the concrete.

In the same scope, measuring the bonding degree between steel fibers and cementitious matrix was a major interest for many researchers. The aim behind such attempts was to identify the ability of steel fibers to increase interfacial bonding and improve the pullout behavior of the fabricated specimens. Babar Ali et al. [19] examined the effect of using steel fibers along with micro silica on the strength properties of cement-based concrete. The main results revealed the fact that low and medium fiber dosages are beneficial in terms of improving strength performance, also, the incorporation of fibers yielded better interfacial bonding in the resulting matrix.

There are many available research attempts on the effect of using brick waste as a binder or as filler within the cementitious matrix, the conducted studies examined these materials separately. However, limited studies are performed based on assessing the existence of fibers within such a matrix.

The main objective of this paper will be to compare the effect of using brick powder within the fiber-reinforced White Cement-based mortar. Compressive and flexural strength results for normal conditions, elevated temperature, sulfate attack, and freeze–thaw cycles will be examined along with the microstructural analysis that includes Scanning Electron Microscopy (SEM) to observe the degree of adhesion between the waste materials and fibers and the White Cement used. Also, X-ray powder diffraction (XRD) analysis will be performed for investigating the relationship between brick powder and White Cement.

2. Materials and methods

2.1. Materials

The main binder used in this study was White Cement (52.5) which was provided by Çimsa Cement Industry and Trade Inc. Clinker is a material produced as a result of the calcination of cement raw materials in the furnace. Free lime (free CaO) content in clinker is an important parameter that determines the quality of cement. The presence of excess free lime may lead to undesirable events such as volume expansion, longer setting time, and lower strength values. X-ray fluorescence technique (XRF) test is used for chemical element analysis of cement material. With this analysis, the concentration of the main oxides is determined. Since XRF spectra do not contain mineralogical information, they show the total Ca concentration in the sample together with free CaO. The titration method or X-ray diffractometry (XRD) test is required to determine free CaO. These tests were carried out by the company from which the White Cement was supplied. According to the results of the analysis, the free lime rate in White Cement is below 2% (1.6%), and it is known to be at the desired level. The waste brick powder was provided from the Manisa region. Table 1 shows the composition and chemical details of White Cement and brick powder. The type of sand used was river sand and its details are listed in Table 2.

Table 1
The chemical composition of White Cement and clay brick powder.

Chemical composition, %	SiO_2	Al_2O_3	Fe_2O_3	TiO_2	CaO	MgO	K_2O	Na_2O	SO_3	Free CaO	L.O.I.
WC	21.60	4.05	0.26	0.35	65.7	1.30	0.35	0.30	3.30	1.60	3.20
CBP	63.6	18.6	9.11	0.35	1.65	1.28	1.82	NA	0.02	NA	11.3

Table 2
Standard limit values and gradation for sand.

Characteristic	Grain size (mm)					
	0.08	0.16	0.5	1.0	1.6	2.0
Remaining (%)	99	87	72	34	6	0
Limit (%)	99 ± 1	87 ± 5	67 ± 5	33 ± 5	7 ± 5	0

Three different types of fibers with the same volumetric percentage were used in this study to examine their bonding degree with the fabricated matrix. The properties of the relevant fibers are shown in Table 3.

Prismatic molds with dimensions of 40 × 40 × 160 mm and cubic molds with 50 mm sides were chosen for this work. Cement, clay brick powder, sand, and fibers were firstly mixed and then the water-superplasticizer solution was added to them, the mixes and series details are illustrated in Tables 4 and 5 and Fig. 1. While [14–16] studies were taken into account on the addition rate of clay brick powder to White Cement, [18–21] studies were taken into account on fiber addition rates. Since the main objective of the study is to observe the behavior of the matrix with different fiber types, then the ratio of fibers was kept constant in all mixes.

A mortar hand mixer was used to gain a homogeneous mix. The mortar was placed into the molds and a vibrating machine was used to eliminate the entrapped air thus reducing the air voids within the matrix. The curing lasted for 28 days and then the specimens were taken out from the curing basin and left for room temperature curing for up to 90 days.

2.2. Test procedure

To evaluate the performance of the specimens under elevated temperatures, the high-temperature test was done for 250 °C, 500 °C, and 750 °C. In the scope of this test, the specimens were firstly put in a drying oven at 105°Celsius for 1 day before the experiment. In the high-temperature oven, the rate of temperature increase was 5 °C/minute up to the required temperature. Then the specimens were kept in the aforementioned elevated temperatures for one hour. Finally, the specimens were left for cooling to avoid the risk of thermal shock which can affect the results. The applied procedure and the choice of temperatures were based on previous investigations [20–21]. The freezing-thawing test was done for 90 cycles and every cycle lasted for 12 h at −20 °C (freezing) and 12 h at + 20 °C (thawing) [21]. Concerning the sulfate attack test, the specimens were left in sodium sulfate solution for 90 days, the concentration of the solution was 5% and the solution was changed every 30 days. On the day before the test, the specimens were taken out of the solution and dried in a drying oven for one hour at 105 °C [22]. After being subjected to the aforementioned tests, experiments on strength loss and weight change for the relevant specimen groups were conducted to better understand the performance of the fabricated composites under durability conditions. Also, microstructural observations were done for the specimens before and after durability tests to examine the nature of the matrix before and after subjection.

Table 3
The properties of the relevant fibers.

Type	Length (mm)	Diameter/ width (mm or μm)	Specific gravity (gm/cm^3)	Nominal tensile strength (MPa)	Aspect ratio
Basalt	12	20 μm	2.73	4100	600
Crimped	50	2.60	7.85	1189	19.23
Copper-coated	6	0.17	7.85	2100	35.29

Table 4
General details of the mixes.

Water/Cement Ratio	0.45
Binder/Filler Ratio	1:2.75
Fiber Percentage	0.4%
Curing Type	Wet Curing

Table 5
Mix proportions of specimens.

Mix ID	Cement (g)	Sand (g)	CBP (g)	Water (g)	SP (g)	FIBER (%)-
WC	450	1237.5	–	202.5	30	–
CBP5	427.5	1237.5	22.5	202.5	30	–
CBP10	405	1237.5	45	202.5	30	–
CBP15	382.5	1237.5	67.5	202.5	30	–
WCCC	450	1237.5	–	202.5	30	Copper-coated steel fiber
WCB	450	1237.5	–	202.5	30	Bazalt steel fiber
WCC	450	1237.5	–	202.5	30	Crimped steel fiber
CBP5CC	427.5	1237.5	22.5	202.5	30	Copper coated steel
CBP5B	405	1237.5	45	202.5	30	Bazalt steel fiber
CBP5C	382.5	1237.5	67.5	202.5	30	Crimped steel fiber

3. Results and discussion

3.1. Mechanical properties

The 28 and 90-day compressive and flexural strength results of 10 series produced within the scope of the study are shown in Figs. 2-3. While a complex series of chemical reactions occurred in the hydration of White Cement, each main component created a separate chemical reaction with water. Calcium silicates (C_2S and C_3S) formed calcium-silicate-hydrate gel ($C_3S_2H_3$) (C-S-H), which was the main binding component of cement, by chemical reaction with water. While the C_3A and C_4AF components affected the initial bonding properties of the cement, the C_3S and C_2S components determined the main bonding properties. White Cement produced higher compressive strength resulting in mortars than Portland Cement. The higher amount of limestone and white limestone and silicate in its composition and the lower amount of Fe_2O_3 and Mn_2O_3, which caused the decrease in the pozzolanic activity of the cement mortar, served a function in the formation of this situation. Thereby, White Cement provided a stronger matrix structure by forming more calcium silicate hydrate gels and filling the capillary pores of the cement mortar more [23–25].

It is important to investigate the mechanical performances of cement-based materials. Strength is the most important factor affecting the performance of building elements produced using cement-based materials. The effect of clay brick powder on compressive and flexural

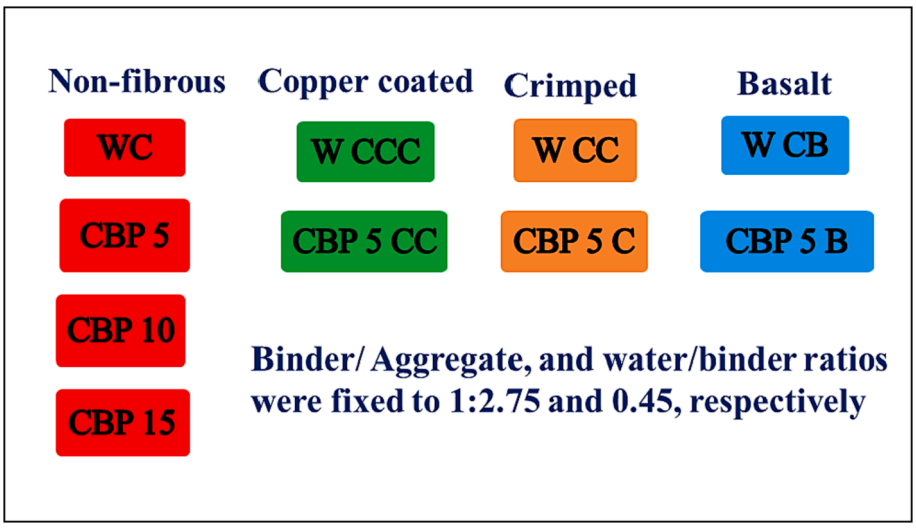

Fig. 1. The components of the binding matrices fabricated in the study.

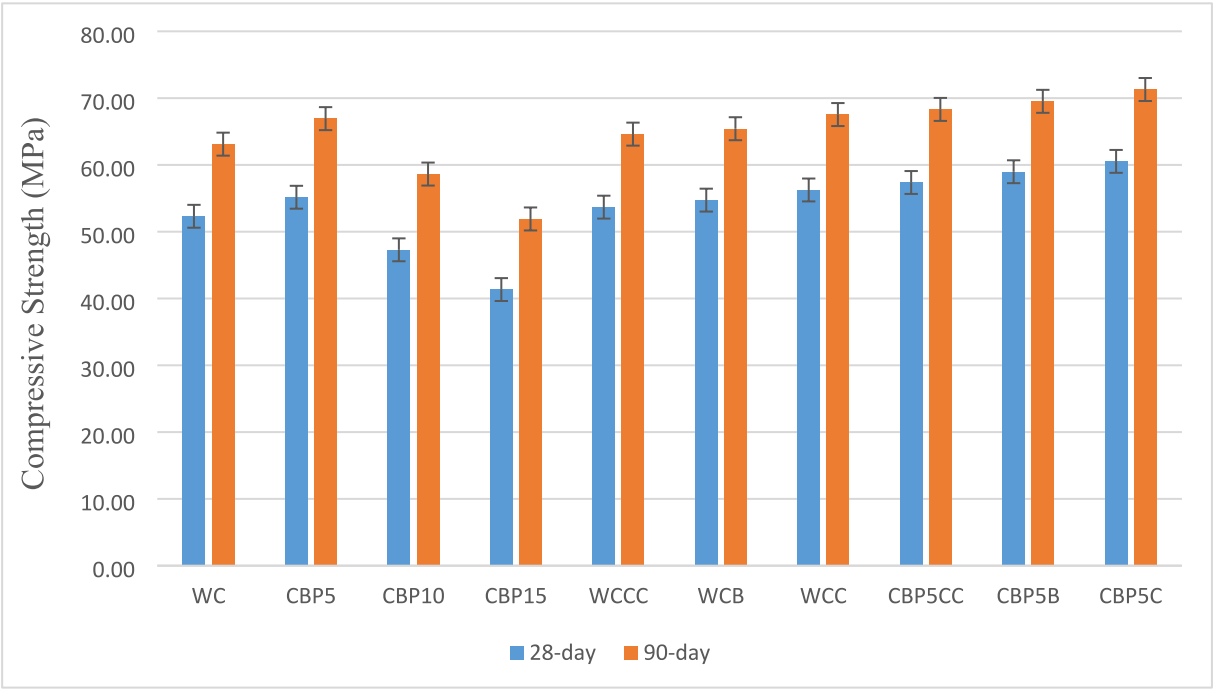

Fig. 2. Compressive strength results.

strength was investigated. When the results of these parameters were examined, it was seen that the use of brick powder up to 5% increased the strength results. The pozzolanic reaction of the brick powder played an important role in this case. The higher SiO_2 and Al_2O_3 content in the brick powder facilitated the reaction with CH, resulting in more production of C-A-S-H and C-S-H gels that bonded the hydration products together. In addition, the formation of a more refined pore network with the brick powder acting as a filler has also been effective in this situation [16,26–29]. The use of brick powder in higher proportions caused a decrease in the relative content of the cement, leading to a decrease in hydration products such as the amount of CH and C-S-H gel. The reduction of CH also reduced the reaction with brick powder. It decreased the strength results due to this situation. The increase in the curing time with 90 days increased the strength results [16]. The 28 and 90-day compressive strengths of sample WC were 52.31 MPa and 63.11 MPa, respectively, while the flexural strengths were 6.79 MPa and 7.88 MPa, respectively. The 28 and 90-day compressive strengths of sample CBP5 were 55.16 MPa and 66.93 MPa, respectively, while the flexural strengths were 7.35 MPa and 8.42 MPa, respectively.

The effect of fibers in the 5% brick powder substitution and the control sample, which gave the highest results, was examined in the strength results. When the structure of fiber-reinforced composites was investigated, it was seen that a small increase in compressive strength occurred in general. The increase was mainly due to the effect of the fibers on crack development. When the cracks advanced and reached the interface, the stress was transferred and with the effect of this situation, the resistance of the fibrous composites to the additional compressive force increased and thus the compressive performance increased. The reasons for the small increase were that the fiber utilization percentage was low and the fibers generally didn't affect significantly the compressive strength. When the effect of fiber length on compressive strength was examined, it was observed that the compressive strength of

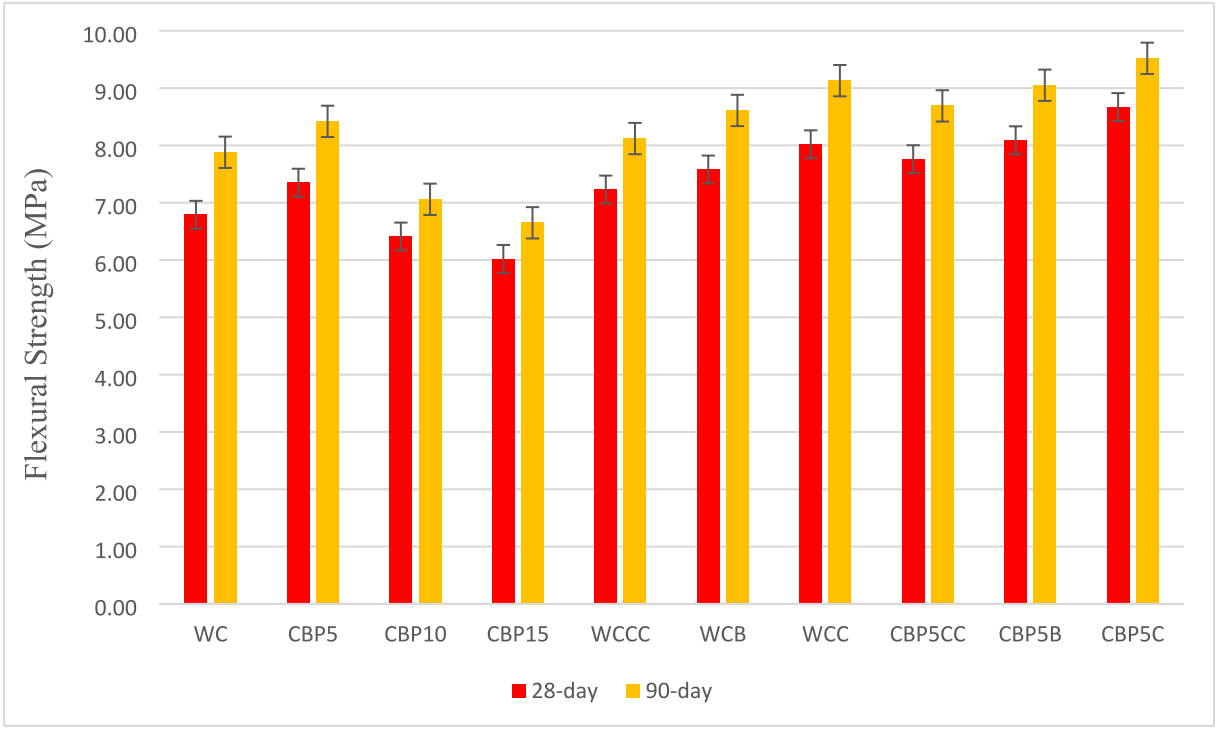

Fig. 3. Flexural strength results.

composites increased with the increase in fiber length. Accordingly, it was determined that the highest results were in the crimped steel fiber reinforcement. In this case, the high density of the crimped steel fiber was also effective. As the fiber length increased, since it reduced the number of voids due to its high density, it helped to improve compressive strength by reducing lateral deformations. Since the copper-coated steel fiber was shorter, it produced the lowest strength among the fibrous mixtures [30–32]. When the effect of basalt fiber was examined, it was determined that it showed a systematic performance. The thin and homogeneous structure of the crystal phases was effective in the targeted physical and mechanical properties of basalt fiber. The targeted microstructure can be achieved by adding a nucleating agent such as ZrO_2, TiO_2, or P_2O_5. Basalt rocks, on the other hand, provided a significant advantage by producing a natural nucleating agent Fe_3O_4 during the melting processes. Therefore, basalt fibers produced from basalt rock, when used in this study, acted as a nucleating agent, helping the crystallization process (the surface topography and roughness of the fibers had a positive effect in the crystallization process) and played an important role in obtaining the targeted microstructure [20,33–34]. According to the flexural strength results, it was found that the increase rates were higher with the fibers. As was known, flexural strengths in fibrous mixtures depended on the type of fiber used, its length and in which direction, and how it was distributed in the blend. Higher flexural strength results were obtained as the crimped steel fiber length was longer and thus fiber slipping became more difficult. Since the copper-coated steel fiber was shorter, it similarly produced the lowest flexural strength among the fibrous mixtures [30–32]. The 28 and 90-day compressive strengths of sample CBP5CC were 57.37 MPa and 68.31 MPa, respectively, while the compressive strengths of sample CBP5C were 60.53 MPa and 71.29 MPa, respectively. The 28 and 90-day flexural strengths of sample CBP5CC were 7.76 MPa and 8.69 MPa, respectively, while the flexural strengths of sample CBP5C were 8.67 MPa and 9.52 MPa, respectively. Although fiber reinforcement improved the mechanical properties, it was disadvantageous if it was added at a high-volume ratio because it both increased the cost and reduced the workability if it was added in excess. Therefore, fibers were added at 0.4% by volume in this study. The addition of copper-coated steel fiber increased the compressive strength between 2.06% and 4.01%, while basalt fiber increased between 3.66% and 6.93%, and crimped steel fiber increased between 6.51% and 9.74%. The addition of copper-coated steel fiber increased the flexural strength between 3.05% and 6.48%, while basalt fiber increased between 7.48% and 11.63%, and steel fiber increased between 13.06% and 18.11%. Mahakavi and Chithra [30] found that adding hybrid hooked end and crimped steel fiber significantly improved the compressive strength, flexural strength, and impact resistance. Celik et al. [20] found an increase in flexural strength between 27.95% and 30.19% with the addition of basalt fiber to geopolymer mortar at a volume of 1.2%. Thus, it was seen that the results found in this study were compatible with the results of other studies.

The microstructure properties of White Cement composites reinforced with brick powder and fibers were investigated with the help of SEM analyses. Due to the analysis, the potential characterization of the substitute materials and fibers in the composite structure was investigated in detail. Also, the interfacial bonding degree was observed among the substitute and reinforcement materials and the main material. SEM micrographs of samples WC, CBP5, CBP5C, CBP5B, and CBP5CC are shown in Fig. 4. If the SEM analyzes were examined in detail, it has been determined that they were in parallel with the compressive and flexural strengths. Increasing the SiO_2 and Al_2O_3 content of 5% brick powder substitution and producing more C-A-S-H and C-S-H gels resulted in a more homogeneous structure compared to the 100% White Cement based sample. Thus, a good bond was formed between the brick powder and the White Cement [26–27]. In addition, the addition of brick powder as a substitute had a positive effect on the bond grade according to sample WC. It was also observed that the interface transition zone (ITZ) between the aggregate and the binder material improved with the contribution of brick dust. Adding fiber reinforcement to the composites increased the ability to stop cracks, creating higher crack resistance and delaying the propagation of microcracks. The higher density and longer length of the crimped steel fiber reduced the number of voids and thus the lateral deformations, resulting in higher cracking resistance. It has been observed that no significant deformation occurred on the fiber surface due to the good bonding of the crimped steel fibers, and it

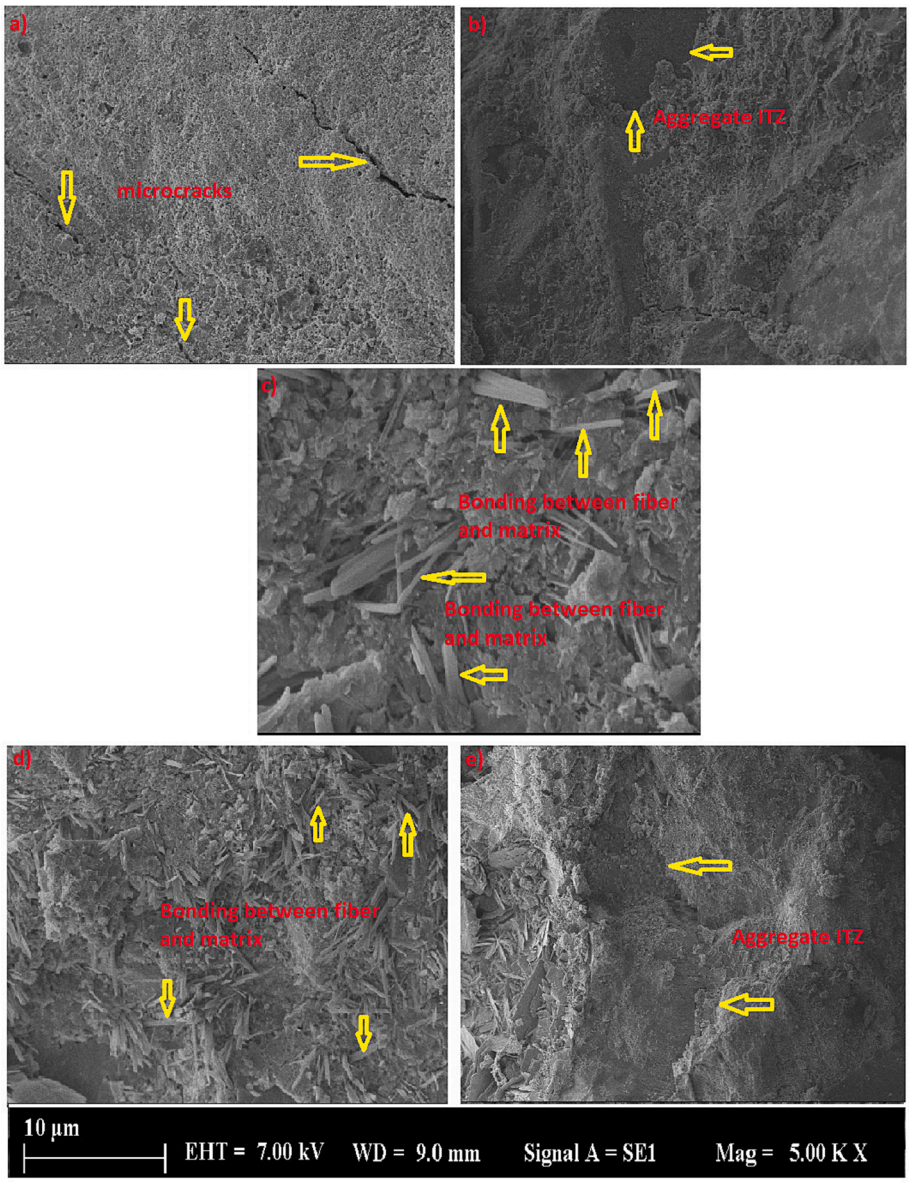

Fig. 4. SEM images of samples: a) WC, b) CBP5, c) CBP5C, d) CBP5B, and e) CBP5CC.

provided more strength increase due to its dense and durable structure. It has been found that basalt fibers also played a role in increasing strength by forming a good bonding degree. Copper-coated steel fibers had a shorter structure and the degree of bonding formed by the fibers was also lower. So, copper-coated steel fiber had a lower strength increase compared to the others due to its shortness [30–34].

In this study, since it was known that the incorporation of fibers into composites didn't cause the formation of crystalline phases, XRD patterns for the produced fiberless mortar samples were investigated. The XRD patterns for the four series (WC, CBP5, CBP10, and CPB15) are given in Fig. 5. While C-S-H (calcium silicate hydrate) gel was observed in the main peaks for all series, portlandite formation was also observed. It was observed that the formation of C-A-S-H (calcium aluminosilicate hydrate) increased with the substitution of brick powder. In this situation, the use of brick powder at the rate of 10% and 15% caused a decrease in the peaks. In the samples examined, it was observed that the peaks were concentrated between 20°-30° 2θ. The compressive strength results of the mixtures also confirmed the microstructural analysis of the formation of the phases [22,26–27].

3.2. *Freezing-thawing effects*

After 90 days were completed, the freezing-thawing test was applied and the losses in flexural and compressive strengths and weight were found. Comparisons of results at test completion with results at 90 days are shown in Figs. 6-8. After 90 cycles, a decrease in strength results was observed. Mortars and concretes had a porous structure containing pores of different sizes ranging from nanometers to millimeters. The structure of these pores was partially filled by water containing different ions, also called pore solution. When mortars and concretes were faced with freezing temperatures, freezing began to occur in the pore water, and ice formation and possible damages occurred with the effect of this situation. These damages were called frost damage or also called internal frost damage. In the explanation of this situation, the expansion effect that occurred in the transformation of water into ice along with the freezing effect had an important place. There were different theories about the actual mechanisms that occurred with the freeze–thaw effect. Hydraulic pressure theory had an important place among these theories [35]. According to this theory, expanding ice formation occurred when water was exposed to a 9% volume increase due to the freezing effect.

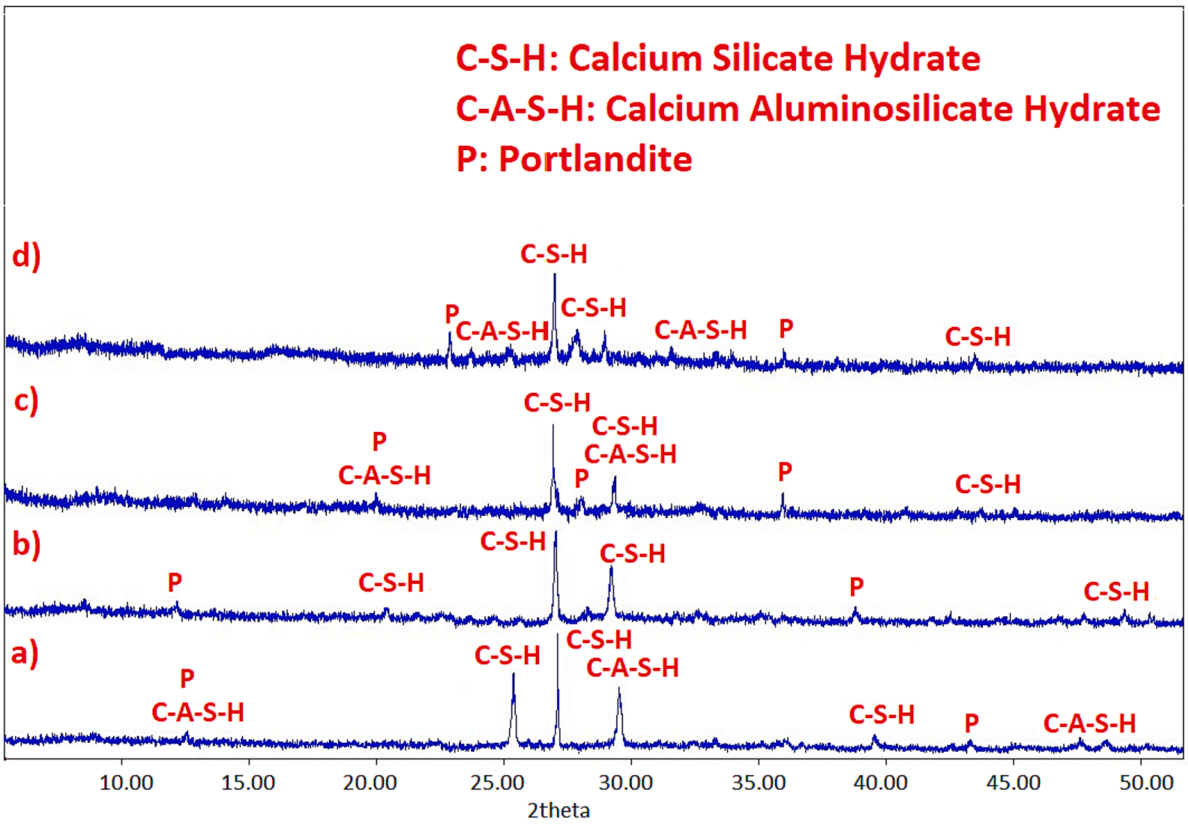

Fig. 5. XRD patterns of samples: a) CBP5, b) WC, c) CBP10, and d) CBP15.

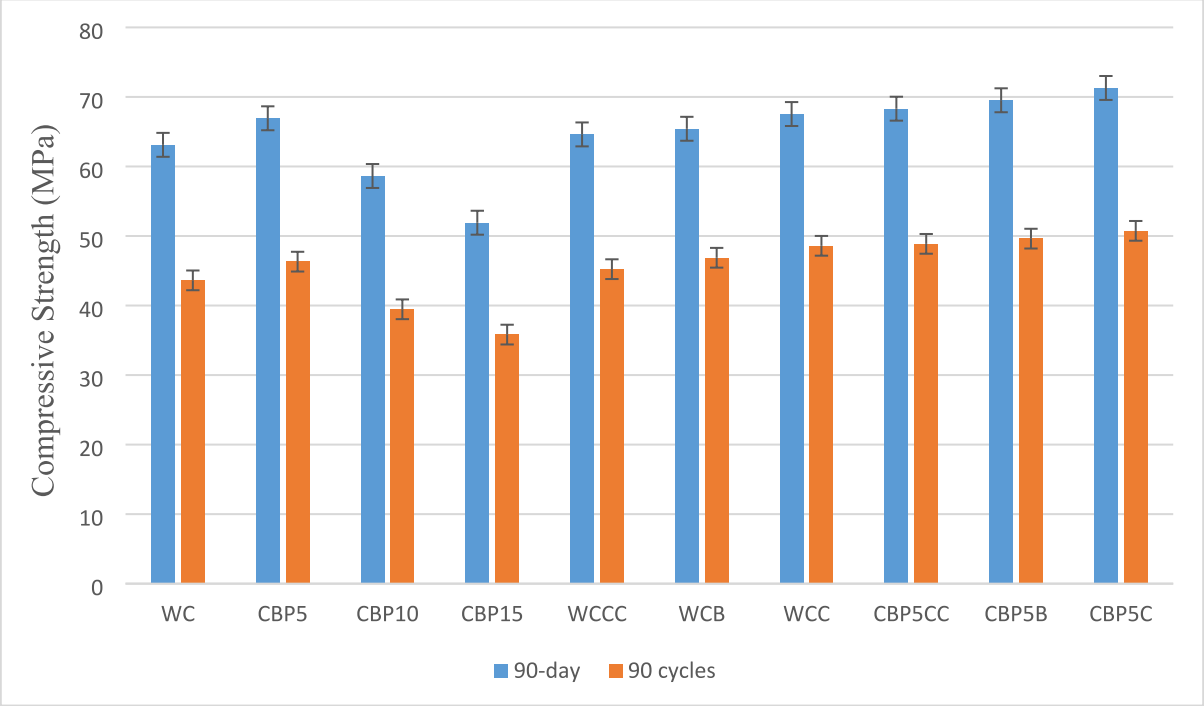

Fig. 6. Compressive strength results after 90 cycles.

While ice formation started in larger pores with capillary pore structure, it expelled the pore water from the frozen pores with the effect of volume increase. Hydraulic pressures could occur depending on the rate of growth of ice, which was a function of the rate of cooling, the level of supercooling before nucleation occurred, and the pore structure of the cement matrix. This caused tensile stresses in the concrete or mortar, and possibly frost damage if it reached tensile strength. According to these explanations, the capillary pressure theory was useful to explain

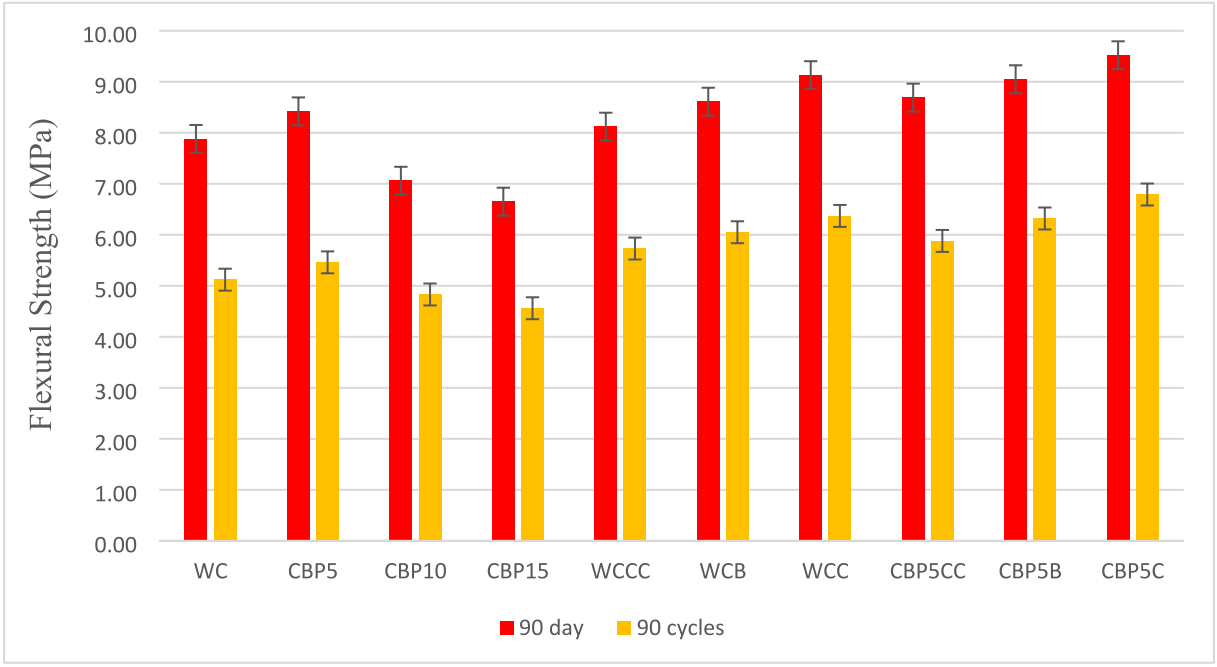

Fig. 7. Flexural strength results after 90 cycles.

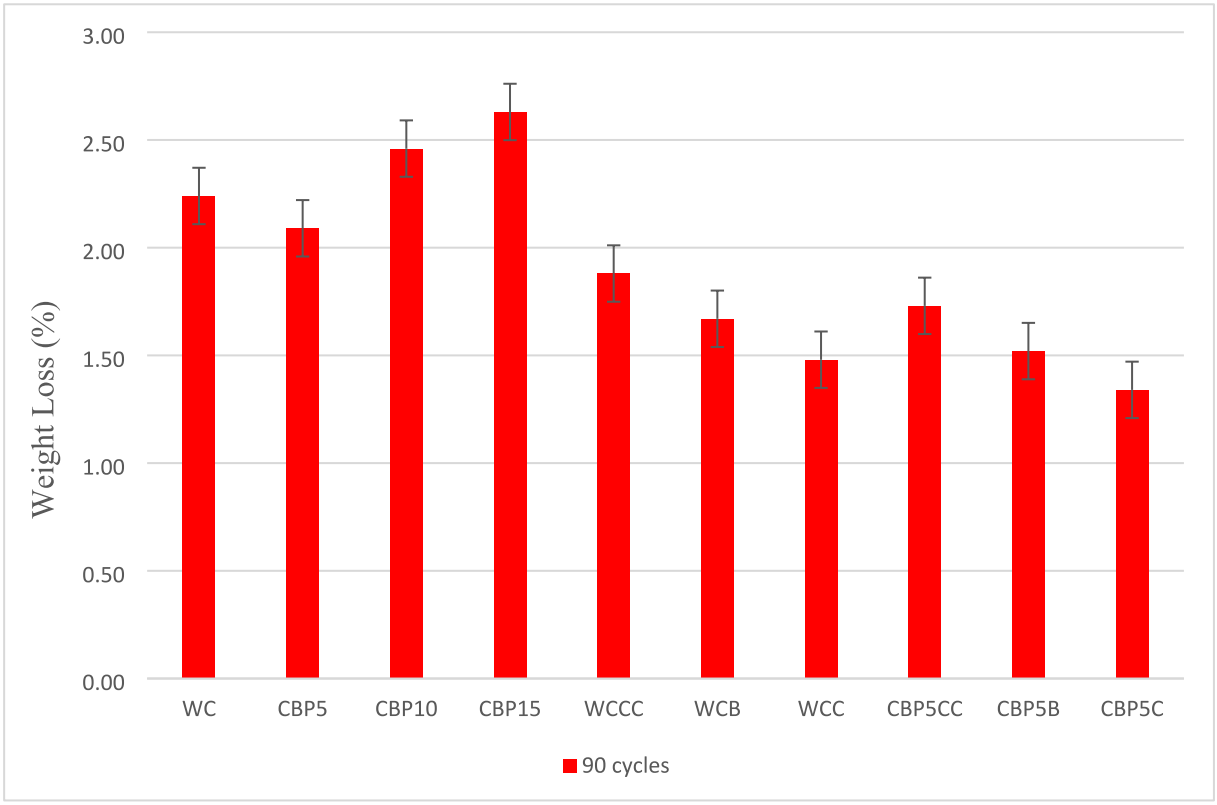

Fig. 8. Weight loss results after 90 cycles.

frost damage caused by the effect of ice formation in the capillary pores. Thus, as the growing ice crystals surrounded the water-filled pores, the resulting fluid pressure caused frost damage. With this effect, there was a decrease in strength results [36–37]. The strength values before the freeze–thaw test effect also determined the degree of micro-cracks. However, the air voids ratio was also a determining factor in this situation. In other words, the moisture content of the sample and the porous network were also effective on degradation. If the sample became saturated and the pore structure could not withstand the stresses due to ice formation, damage began to occur. Freeze-thaw damage was primarily affected by excess water inside and on the surface of assemblies. There were two types of cracks: surface spalling and internal

cracking. Surface spalling was caused by the effect of repetitive water on both vertical and horizontal surfaces, and the effect of this situation kept the surfaces wet for a long time. While freezing occurred, the outer layer of the material was broken down to the depth of water penetration. Spalling on the concrete or mortar surface exposed the softer and porous inner layers below that were more susceptible to freeze–thaw action, leading to further deterioration with repeated cycles. Internal cracking occurred because of internal cracks and voids being exposed to freezing by filling with water. Unlike surface spalling, it started in the inner structure and cannot be seen visually. Both types of cracks increased with the increase in the cycle number. So, freezing damage due to the repetition of freeze–thaw cycles was caused by the gradual expansion of the cement paste, internal cracking, and surface scaling with the effect of moisture. Distortions did not have to occur simultaneously. Due to these conditions, the increase in the number of air voids increased the strength losses [38]. The use of active pozzolans provided satisfactory behavior against freeze–thaw cycles without creating a specific air void requirement. Because of this situation, the use of 5% brick powder also increased the resistance against freeze–thaw cycles. Higher rates, on the other hand, caused an increase in shrinkage cracks, leading to a decrease in resistance to cycling [26–27]. The positive contribution of the fibers before the freeze–thaw test resulted in higher post-test results [30–34]. At the end of the freezing-thawing test, the compressive strength of sample CBP5C was 50.74 MPa, while the flexural strength was 6.79 MPa. At the end of the 90 cycles of the freeze–thaw test of sample CBP15, the compressive strength was 35.82 MPa, while the flexural strength was 4.56 MPa. The temperature-related deterioration values in the flexural strength of mortars were higher than the compressive strength. In the three-point bending strength test, oblique cracks were more common, while in the compressive strength test, cracks occurred more parallel to the compressive load. Therefore, flexural strength was more sensitive to the development of internal structural defects (propagation of cracks) than compressive strength and decreased more with embrittlement under the influence of high temperature [39].

When the weights of the samples were examined, it was seen that the losses from the freeze–thaw cycle were low. The number of cycles was effective in weight loss. The moist content in the environment where the test was carried out enabled some of the gaps to be filled. Following the micro-crack formation, the moist environment provided some filling of the voids. Thus, a movement also occurred towards the inside parts with the effect of the humid environment. It was observed that micro-cracks and their deterioration increased with the number of cycles. Thus, after the increase in the cycle numbers, surface calcification and peeling also increased, resulting in weight loss. The use of brick powder up to 5% and fiber effects resulted in a more stable microstructure and lower weight loss. Weight losses after freeze–thaw cycles were found to be between 1.34% and 2.63%. While the lowest value in weight loss was observed in sample CBP5C, the highest value was observed in sample CBP15. Cement hydration and lower void ratio were effective in this situation. The stronger microstructure prevented micro-cracks while limiting weight loss. Thus, weight losses and strength results showed parallelism [39–40].

In the follow-up of the freeze–thaw test, the changes on the surface of the samples were carefully examined. When the surfaces were examined after 90 cycles, no significant damage was detected. The protection of the surfaces indicated that the damages remained at the micro-crack level. After the water expansion exceeded 9%, the force generated by the hydraulic pressure effect exceeded the tensile force, although small micro-cracking occurred [21]. The appearance of the specimens following the test is shown in Fig. 9.

micrographs of samples WC, CBP5, CBP5C, CBP5B, and CBP5CC after 90 cycles of freeze–thaw are shown in Fig. 10. When the SEM images were examined, microcrack formation was detected. The change of the interface between the gel and the cement due to freeze–thaw effects facilitated the propagation of micro-cracks, resulting in the formation of a defective area. Despite this situation, microcracks formed a network by connecting. This has been effective in the low rate of damage to the matrix structure. The slow progression of microcracks also limited the strength drops. Due to the high SiO_2 and Al_2O_3 content of 5% brick powder substitution before the test, C-A-S-H and C-S-H gels were produced more, resulting in a more homogeneous structure compared to the 100% White Cement based sample. This situation improved the bond grade relatively. Although microcracks were formed in the interface transition zone (ITZ) between the aggregate and the binder material, it

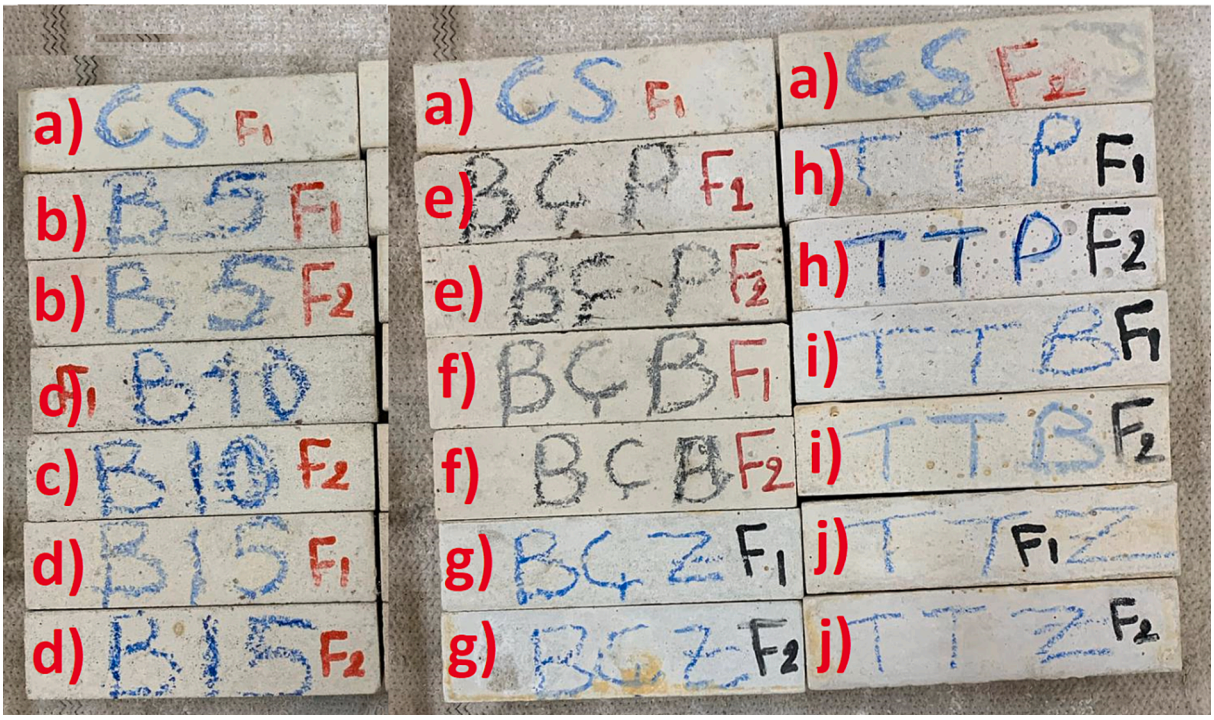

Fig. 9. Visual inspection after 90 cycles: a) WC, b) CBP5, c) CBP10, d) CBP15, e) WCCC, f) WCB, g) WCC, h) CBP5CC, i) CBP5B, j) CBP5C.

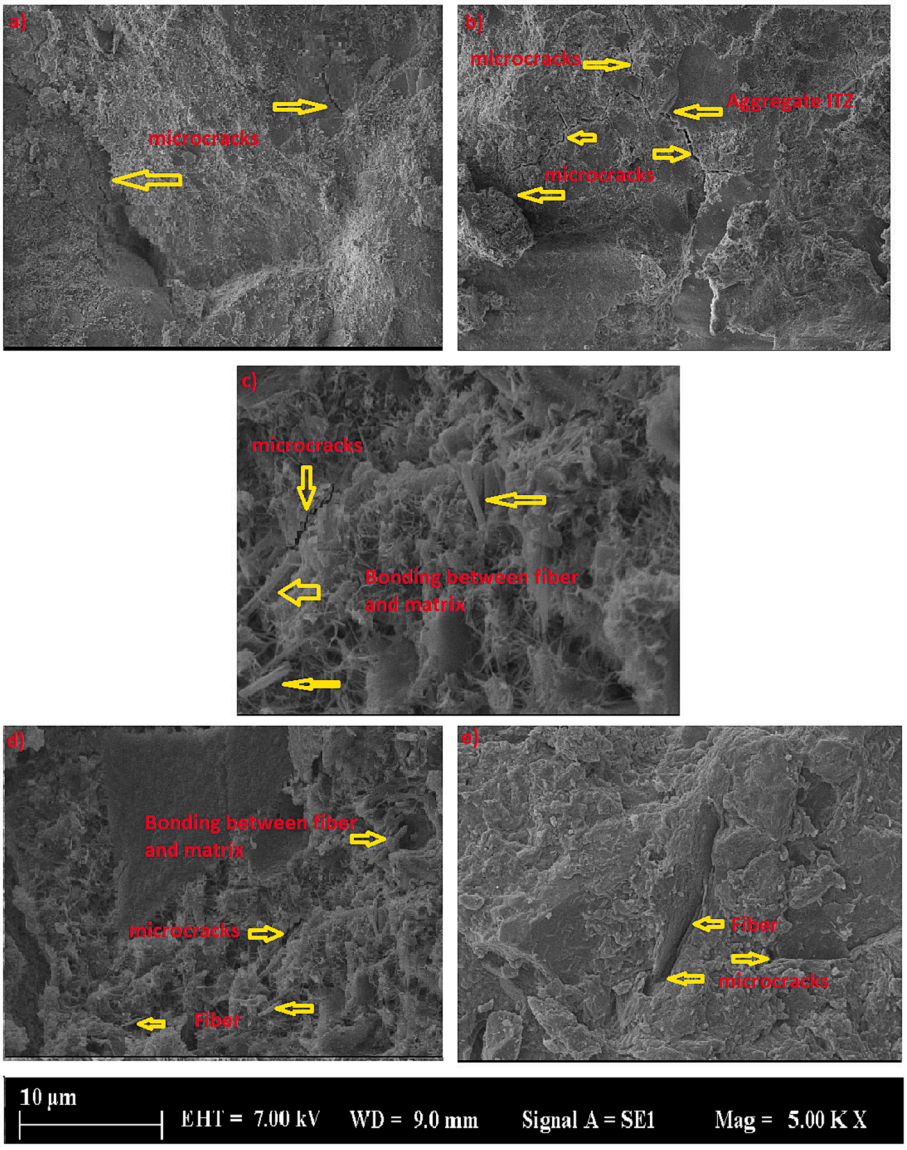

Fig. 10. SEM images after 90 cycles: a) WC, b) CBP5, c) CBP5C, d) CBP5B, and e) CBP5CC.

was observed that they remained at a limited rate with the contribution of brick dust [26–27]. In the case of fiber reinforcement in the composites, it increased the crack resistance and reduced the formation of micro-cracks. In particular, the crimped steel fiber reduced micro-cracks due to its longer and denser structure. The increase in the compressive strength of the crimped steel fiber was due to the behavior of the fibers against the progressive cracks. Progressive cracks were prevented by experiencing a blunting process and stress loss when encountering the fibers. At the same time, with this blunting method, the mortar samples were exposed to a higher compressive load and the compressive strength values were increased compared to the fiberless samples. This was also supported by SEM micrographs. Basalt fibers also increased strength values by resisting cracks. Copper-coated steel fibers had a shorter structure, resulting in a decrease in bonding degree, resulting in less strength increase. So, copper-coated steel fiber showed lower strength compared to other fiber types [30–34]. As a result, composite specimens showed significant resistance against 90 cycles. The related results were consistent with the results of other studies [39–40].

3.3. *High-temperature effects*

With the application of three different temperatures (250, 500, and 750 °C) to the samples, the losses in flexural and compressive strengths and weight according to the 90-day are seen in Figs. 11-13. With the detailed examination of the results, decreases in strength and weight were observed. The decrease in all mechanical properties increased at a rate higher than 500 °C. Existing thermal reactions were effective in this situation. As the free water evaporated with the effect of the reactions, dehydration occurred in the sample matrix structure [41–43]. Increasing temperatures after 600 °C also increased the reduction rates. The steam effect was effective in strength losses after 500 °C. While the steam effect was the main reason for the strength loss, the existing water in the sample turned into steam with the increase in temperature. This situation can be explained by giving more detail. As the water boiled with the increase in temperature, some molecules reached sufficient kinetic energy to escape from the spaces on the surface without returning to the liquid state. With the increase in heating, there was an increase in excitations and this situation increased the number of molecules that caused the fluid loss. When water was heated to its boiling point, steam bubbles formed in it and tried to rise to the surface.

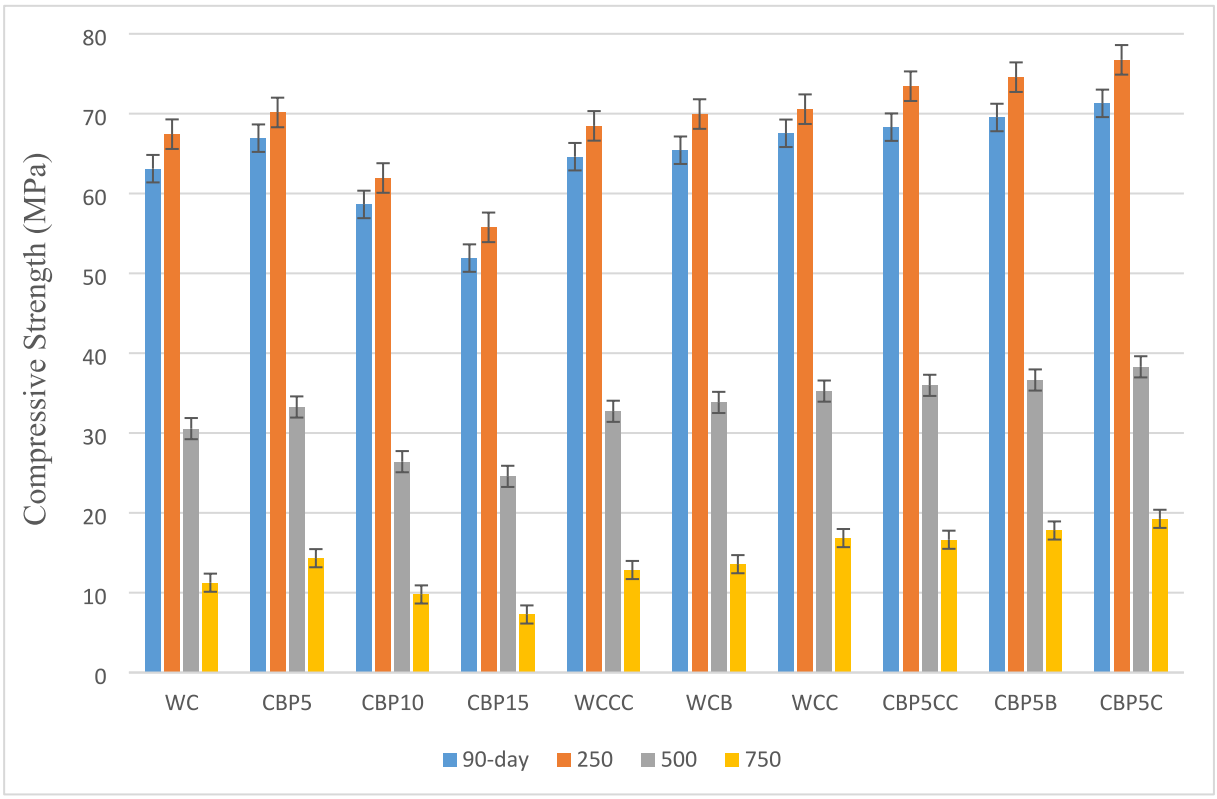

Fig. 11. Residual compressive strengths with the high temperatures.

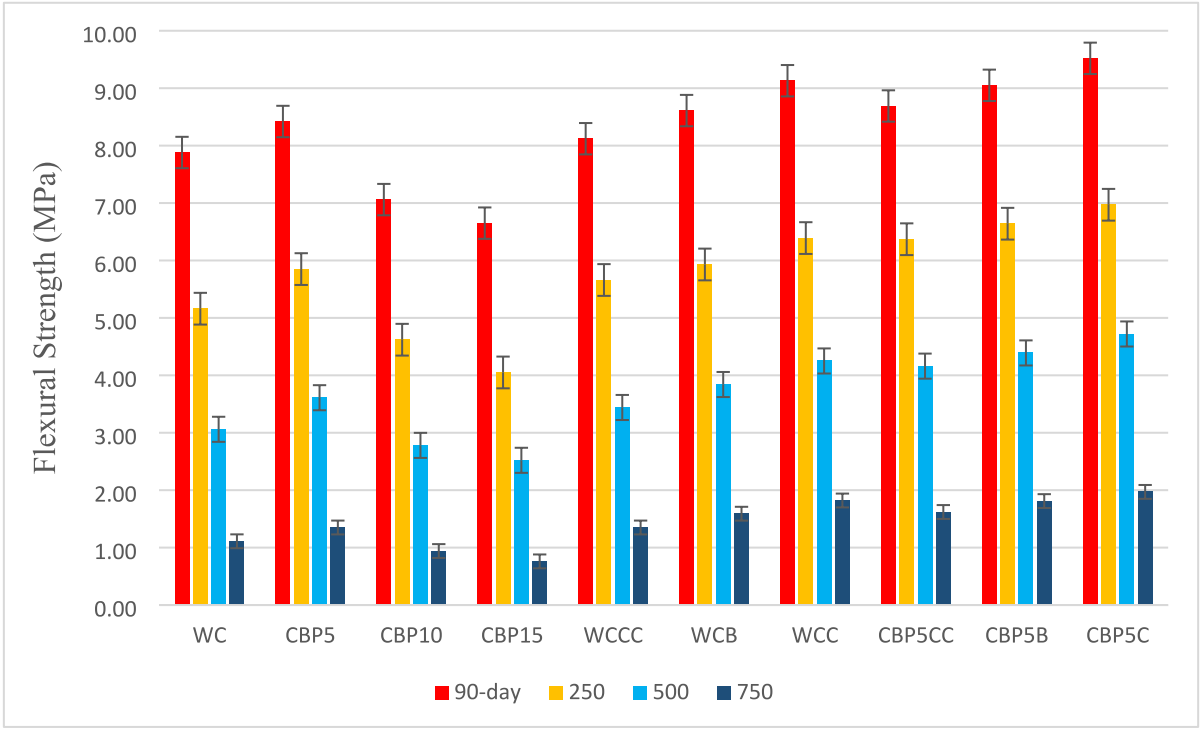

Fig. 12. Residual flexural strengths with the high temperatures.

Considering the molecular arrangement of vapors and liquids, it can be seen that the density of the vapor was less than that of water because the steam molecules were further apart from each other. This allowed the space just above the liquid surface to be filled with less dense steam molecules. Water evaporated freely when more molecules were leaving the liquid surface than those re-entering. At this stage, it reached the saturation temperature as it became saturated with heat energy. Adding more heat caused the water to form saturated steam. Water and steam

Fig. 13. Weight-loss results after high-temperature effects.

can exist at any pressure, both at the saturation temperature. The temperature above the saturation temperature was called the superheat of the steam, while the heat energy increased with the additional heat. This situation increased the pressure, causing an increase in the saturation temperature, thus increasing the losses. After 100 °C, the internal pressure tended to increase continuously. After the steam pressure limit was crossed, condensation in the matrix structure started with very little permeability. With this situation, the resistance of the sample to thermal effects decreased. Then, thermal cracks occurred on the sample surface. The weight losses increased due to water evaporation in the matrix. While cracks increased with the effect of thermal shrinkage, this situation also triggered strength and weight losses. High temperatures also created thermal incompatibility in the paste-aggregate interface transition region, increasing micro-crack formation [44]. The calcium silicate hydrate (C-S-H) gel structure was exposed to more crystallization due to the increase in temperature. The crystallization stress produced thermochemical decomposition in the crystal lattices. Renewal of crystallization had a negative effect on ductility and strength conditions. The thermal incompatibility that occurred after the degradation of homogeneity caused an increase in micro-crack formation.

With these effects, the importance of a strong cement structure increased. The strong character of the sample structure resulted in less thermal gradient by dissipating the heat faster. With these cases, splits and thermal cracks became more limited. It was seen that the flexural strength was affected at a higher rate in the face of high temperatures. While increasing temperatures allowed cracks to propagate, this triggered the growth of the pore structure and the formation of microstructural defects. Flexural strength was also significantly affected by microstructural defects [45]. In addition to these, negative effects on workability and pore properties also played a role in losses. If the general evaluation of the high-temperature results was made, it was seen that the post-test results were similar to the situation before. The 5% brick powder substitution facilitated the reaction with CH, due to pozzolanic reactions, which was the ratio of SiO_2 and Al_2O_3 in its content and provided the formation of more hydration products. In this way, it played a role in the development of strength by reducing air voids and producing more C-A-S-H and C-S-H gels. However, using a higher rate led to a decrease in resistance due to shrinkage cracks [26–27]. Since the crimped steel fiber was longer than the copper-coated steel fiber, it created a stronger bond, increasing the resistance to high temperature. Basalt fiber also showed a systematic performance and showed superior high-temperature resistance [30–34]. When the high temperatures of 250, 500, and 750 °C were applied, the compressive strength values of sample CBP5C were 76.74 MPa, 38.29 MPa, and 19.25 MPa, while the flexural strengths were 6.97 MPa, 4.72 MPa, and 1.97 MPa. When the high temperatures of 250, 500, and 750 °C were applied, the compressive strength values of sample CBP15 were 55.76 MPa, 24.57 MPa, and 7.27 MPa, while the flexural strengths were 4.05 MPa, 2.52 MPa, and 0.76 MPa.

After the test, the weight values decreased as well as the strength values. These losses increased significantly with temperature. The water evaporation and dehydration in the cement matrix formed by the heat effect caused the microstructure to be damaged, and weight losses occurred due to these conditions. The growth of the pore structure also served a function in this situation. In this case, weight loss increased with additional voids. Weight losses consisted of three separate stages. When the cement was hydrated, 50–70% C-S-H (calcium silicate hydrate) was formed as the main chain product, 10–15% ettringite (calcium sulfoaluminate) and 20–25% CH (calcium hydroxide or “lime”) were formed. While C-S-H played the main role in increasing the strength of concrete, CH couldn’t build strength but had efflorescence and poor chemical resistance. When the high temperature was applied to cement paste, portlandite (calcium hydroxide) and calcium silicate hydrates were subject to decomposition. C-S-H gel with an amorphous structure was subject to degradation over a wide temperature range. While C-S-H gel was exposed to dehydration in the temperature range of 100 °C–400 °C, it was observed that it started to decompose at 560 °C and it was reported that it turned into C_2S and C_3S after 750 °C. Weight loss at 300 °C may occur as a result of evaporation of capillary water in macro capillary pores, evaporation of gel water from gel pores of cement paste, and partial dehydration of C-S-H. Weight loss occurred as a result of dehydration of portlandite in cement paste at 450 °C. Between 600 °C and 750 °C, weight loss occurred as a result of dehydration of the residual portlandite and C-S-H and decomposition of calcite. Since the polymeric main and side chains and excess water molecules changed under the effect of high temperature, its role in the formation of weight

loss has been explained in the theories related to the high-temperature effect. Following these stages, the weight losses increased. The higher the temperature values, the higher the losses. Interfacial disturbances between the matrix and the aggregate also led to increased weight loss and these situations were seen in Fig. 15 [46–48]. The use of 5% brick powder and the use of fibers reduced micro-cracks, resulting in an increase in density and a decrease in losses [49]. After applying the effect of temperature at 250 °C, the weight losses were between 1.56% and 2.66%, after 500 °C it was between 4.31% and 5.24% and after 750 °C it was between 6.38% and 7.47%.

Visual inspection was observed for the samples after the 750 °C temperature test was applied. The resulting changes on the surface are shown in Fig. 14. The photographs were taken 60 min after the high-temperature test and the samples were taken out of the oven. Depending on this situation, while the effects of high temperature had a low effect on the sample surface, they showed more effect on the microstructure. When the photographs were carefully examined, the color change was observed on the surfaces after 750 °C. Damage to the main chains in the cement mortar increased the sample surfaces' tendency to become rough and slightly brittle. Nevertheless, cracks on the surfaces were limited. According to this situation, the samples maintained their stability [41–43].

The changes in the composite samples after the application of 750 °C temperature were examined with the help of SEM analysis. SEM micrographs of samples WC, CBP5, CBP5C, CBP5B, and CBP5CC after high temperature are shown in Fig. 15. It has been observed that post-high temperature signed of progress were in microcracks. In this case, the effective factors were the decomposition in the matrices, phase transformations, and weight losses. Under the influence of the conditions, there was an increase in structural defects, and subsequently, the density of defect formation increased. With the increasing defects, a more porous structure was formed. Thus, air voids were formed along with microcracks. The addition of 5% brick powder increased the Al_2O_3 and SiO_2 content, creating more C-A-S-H and C-S-H gels, and a more homogeneous structure was achieved compared to the 100% White Cement based sample. Improvement in bond grade advanced with this condition [26–27]. Also, micro-cracks were observed especially in the aggregate and binder interface transition zone (ITZ) after the effect of high temperature, but this situation remained at a low rate due to the effect of the brick powder. In addition, although cracks and air voids were formed, the effect of the fibers also reduced the stress loss by creating a blunting effect. The crimped steel fibers have created a more resistant structure due to their denser and longer structure. Basalt fibers also reduced losses by resisting cracks. Copper-coated steel fibers, on the other hand, had a shorter structure, thus lowering the bonding degree compared to other fibrous samples [30–34]. Despite these situations, which occurred in parallel to the compressive strength decrease, it was seen that the composite structure was preserved [41–43].

For this work, XRD analysis was performed to examine the crystal phases of fiberless composites after the high-temperature effect because there was a limited effect of fibers on crystalline phases. The XRD patterns for the four series (WC, CBP5, CBP10, and CBP15) are shown in Fig. 16. It was observed that the X-ray diffraction densities were lower as a result of the high-temperature effect of 750 °C. The high-temperature effect caused the decomposition effect of the amorphous hump to lower angles after 750 °C, and probably caused the rearrangement of atomic

Fig. 14. Visual inspection after 750 °C: a) WC, b) CBP5, c) CBP10, d) CBP15, e) CBP5CC, f) CBP5B, g) CBP5C, h) WCCC, i) WCB, j) WCC.

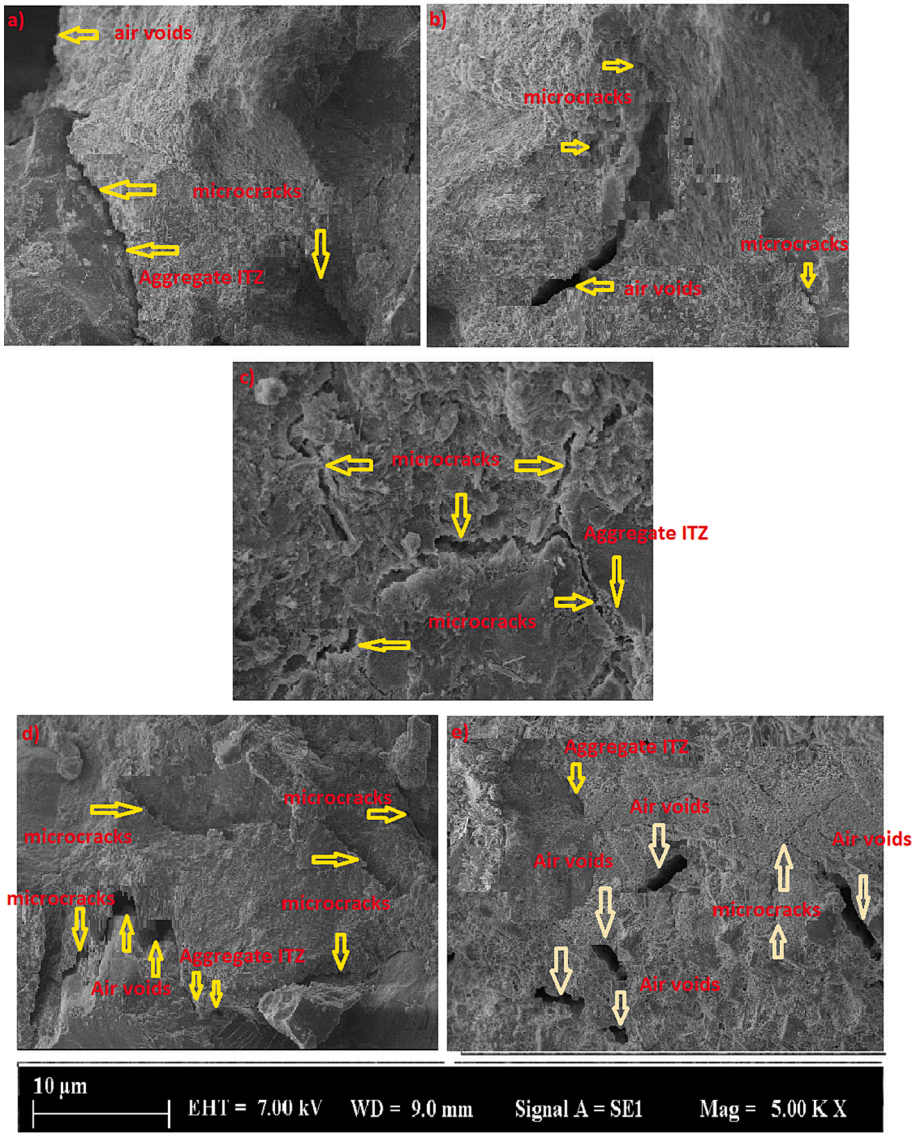

Fig. 15. SEM images of samples after 750 °C: a) WC, b) CBP5, c) CBP5C, d) CBP5B, and e) CBP5CC.

species in the structure of the C-A-S-H and C-S-H gel. On the other hand, the use of brick dust of up to 5% created a more homogeneous structure by forming C-S-H and C-A-S-H gels before the high-temperature effect, resulting in higher resistance. The addition of brick powder at higher rates resulted in lower X-ray diffraction densities.

3.4. Sodium sulfate effects

With exposing sodium sulfate to the samples, the losses in flexural and compressive strengths and weight gain according to the 90-day are given in Figs. 17-19. Significant cracks and porosity increase occurred as a result of the reaction of sulfate crystals formed by the effect of sulfate attack with calcium expansion products. The erosion effect caused by the diffusion of Na into the matrix caused a loss of strength. The presence of microcracks as a result of ettringite and gypsum formed in the pores, as well as the transition of alkalis from the sample matrix to the solution, played an active role in this case. In addition, keeping the samples at 105 °C for 24 h before testing facilitated more effective absorption of sulfate solutions. In this tendency, temperature facilitating absorption by affecting the voids ratio more played a role [50–53].

When the results were examined in detail, it was determined that the samples with low performance in compressive strength before the sulfate effect were the samples that were most affected by the sulfate solution, and therefore they suffered the highest loss of compressive strength. The samples showing high performance in compressive strength underwent less weight change. Because the substituted samples with the highest compressive strength results were more homogeneous and less porous, less solution filled the pores and there was less change in weight. In the results related to the compressive strength, it was observed that the sulfate had less effect on the mixture of White Cement and 5% clay brick powder than the mixture with %100 White Cement, and the compressive strength was higher. By facilitating the reaction with CH with the ratio of SiO_2 and Al_2O_3 in its content, it increased the formation of hydration products and played a role in the development of strength by forming more C-A-S-H and C-S-H gels. However, at higher rates, it caused a decrease in resistance due to shrinkage cracks [26–27]. The addition of 10% clay brick powder had less compressive strength than the White Cement mixture without additives, while the sample with 15% clay brick powder addition had minimum compressive strength.

An improvement in compressive strength was observed after the fibers were added to the White Cement mixture. The crimped steel fiber addition had the highest compressive strength among other fiber types added to White Cement, followed by the basalt fiber added sample. The

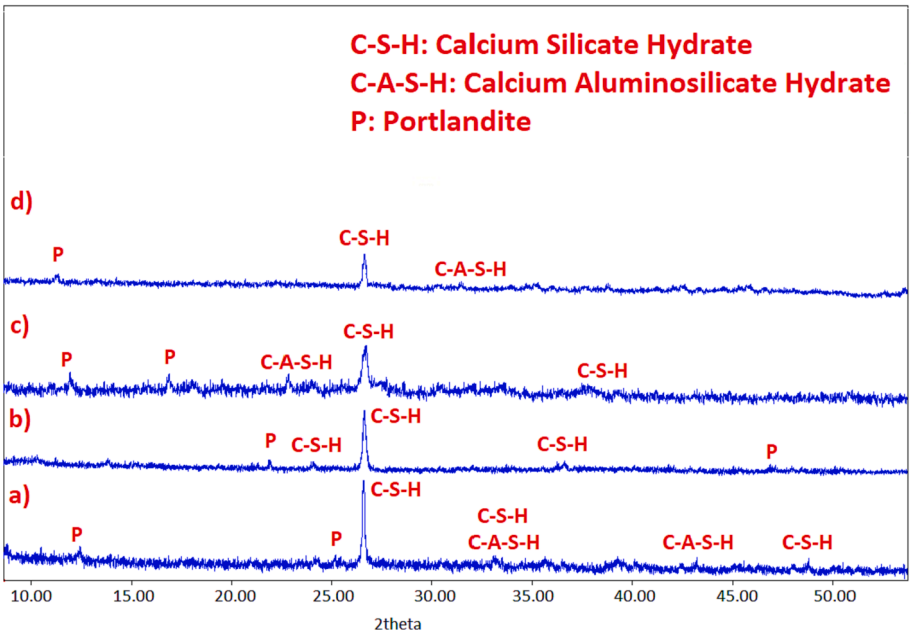

Fig. 16. XRD patterns of the samples after 750 °C: a) CBP5, b)WC, c) CBP10, and d)CBP15.

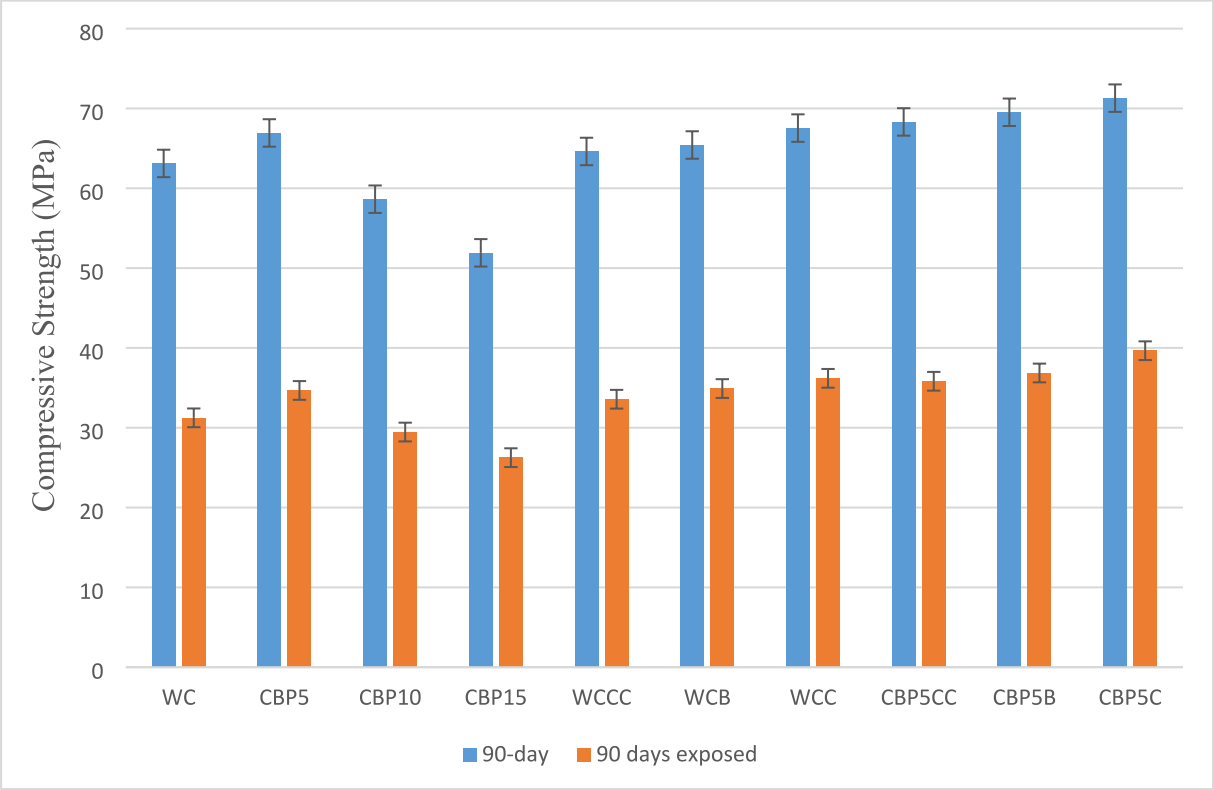

Fig. 17. Compressive strengths result after 90 days exposed to sodium sulfate.

copper-coated steel fiber sample came last in the ranking. The longer crimped steel fibers and the systematic performance of basalt fibers were factors in the ranking [30–34]. When the fibers were added to the samples to which 5% clay brick powder was added, an improvement was found in the compressive strength and the highest compressive strength results were obtained compared to the other samples. The copper-coated steel fiber added sample came last in the ranking.

When the results were examined in detail, it was determined that the samples with low performance in flexural strength before the sulfate effect were the samples that were most affected by the sulfate solution, and therefore they suffered the highest flexural strength loss. According to the results, it was seen that the flexural and compressive strengths showed parallelism. The main reason for the decrease in strength was the micro-crack formation due to the effect of ettringite and gypsum formed in the pores due to the effect of sodium sulfate [50–53]. According to the results of the sulfate test, it was observed that the weights

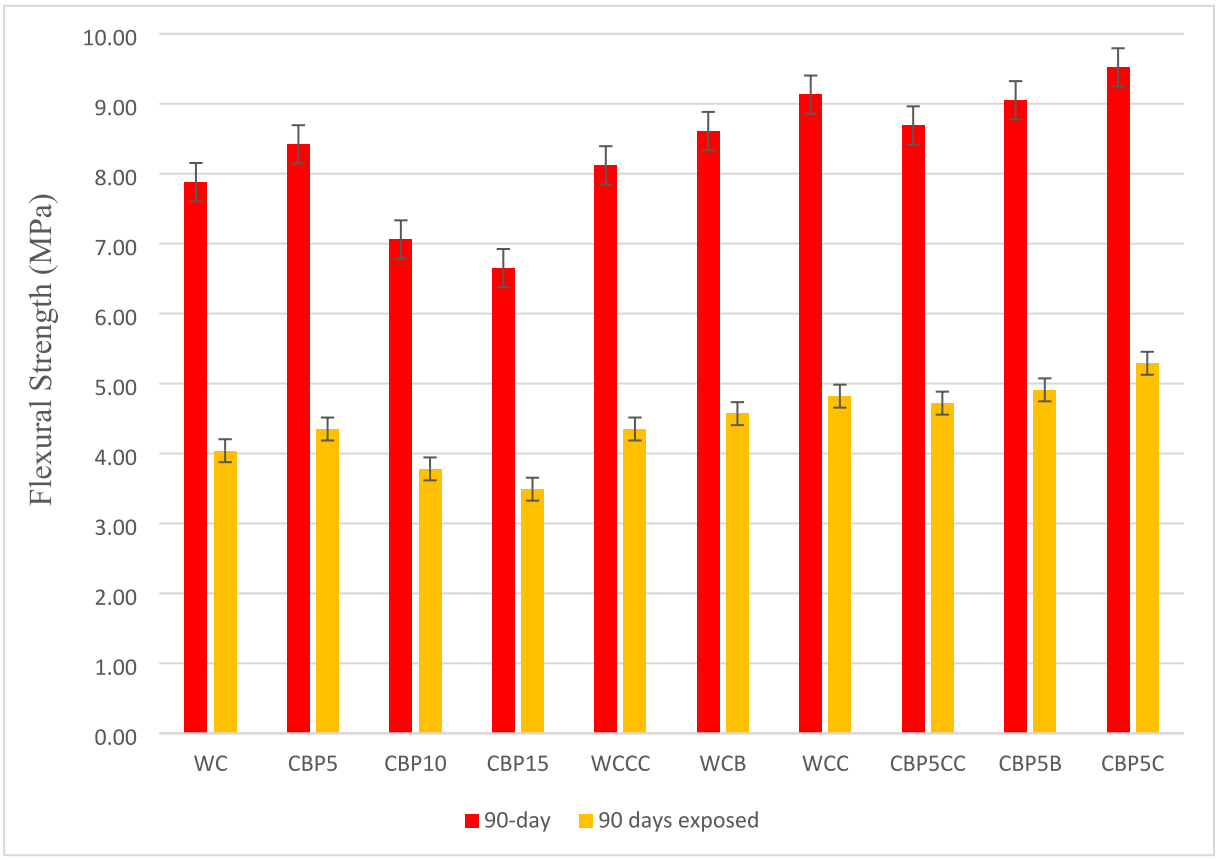

Fig. 18. Flexural strengths result after 90 days exposed to sodium sulfate.

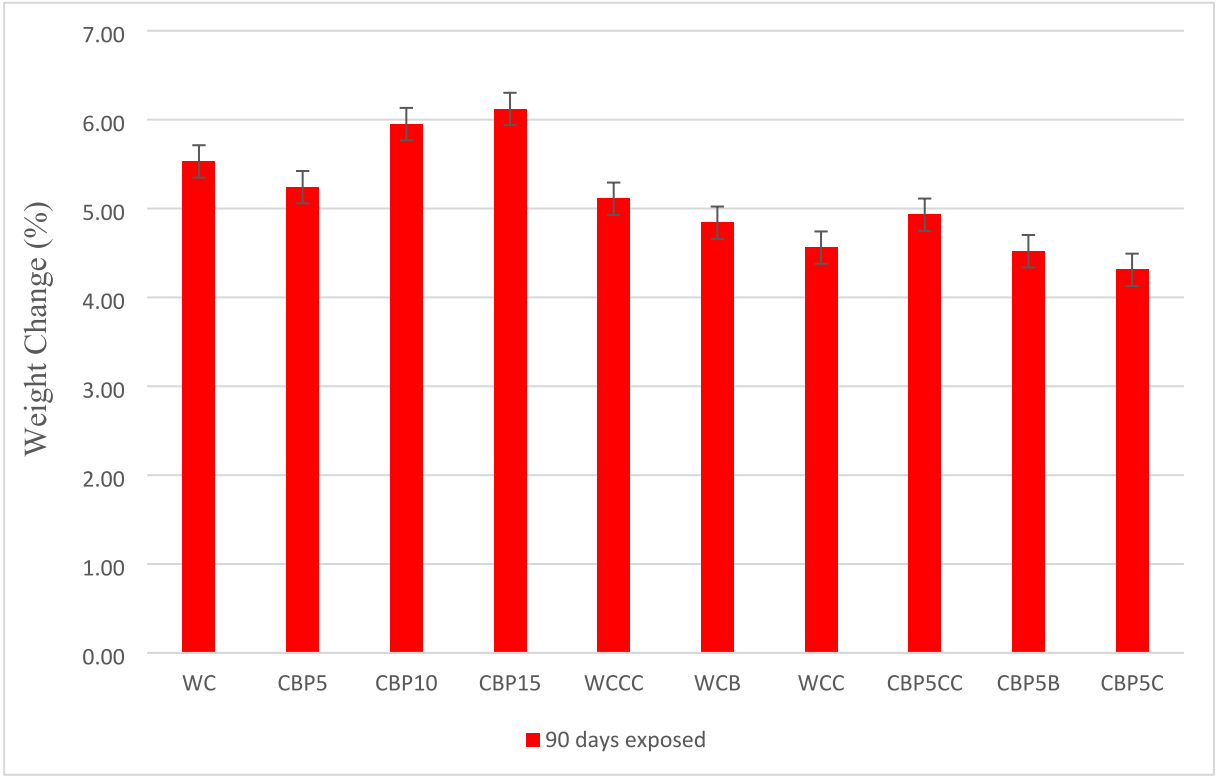

Fig. 19. Weight change results after 90 days exposed to sodium sulfate.

of the samples increased compared to before the sulfate solution test. This was due to the solution filling the pores of the samples. Thus, the weight of the samples increased. In addition, drying the samples in the oven before the sulfate test was also effective in the weight increase. While it was noticed that there was a variation in the increase in the weight of the samples, it was seen that the substitution rates affected this situation. It was found that the variation was in parallel with the strength results.

The visual condition of the samples after exposure to sodium sulfate was examined. When the surface of the samples was examined, softening was observed, while this situation was more pronounced in the corners of the fiberless samples. As the brick powder percentage increased, the attenuation increased even more. While softening decreased in fibrous samples, small cracks were observed on the surface. This situation created a parallel situation with the losses in compressive strength. However, the samples did not lose their stability against the effect of sulfate [22]. The visual appearance of the samples against the sodium sulfate effect is shown in Fig. 20.

SEM micrographs of samples WC, CBP5, CBP5C, CBP5B, and CBP5CC are shown in Fig. 21 after sulfate exposure. Micro-cracks were seen in SEM images of cementitious composites. It has been observed that the cement-gel interface turned into a defective area with the effect of sodium sulfate, facilitating micro-crack propagation. The formation of ettringite and gypsum in the pores created microcracks due to the sodium sulfate attacks. Network formation by the bonding of microcracks resisted this situation. Therefore, the damages remained low in the matrix structure. In addition, slow-growing microcracks also slowed down the strength drops. The use of 5% brick powder before the sulfate effect provided an increase in the ratio of SiO_2 and Al_2O_3 and provided a more homogeneous structure by strengthening the C-A-S-H and C-S-H gels. With the effect of this situation, the bond degree was strengthened. Although the interfacial transition zone (ITZ) between the aggregate and the binder material took a micro-cracked structure due to the sulfate effect, the more homogeneous structure of the brick powder limited the cracks [26–27]. The increase of cracking resistance in composites with the effect of fibers reduced micro-crack formation. The crimped steel fibers had a denser and longer structure, reducing micro-cracks. Basalt fibers also showed resistance to cracks, increasing the resistance compared to the fiberless samples and compared to the copper-coated steel fiber. The resistance increase in the copper-coated steel fiber was the lowest [30–34]. The results against the sulfate effect were consistent with the relevant studies [52–53].

4. Conclusions

For this paper, White Cement was substituted with brick powder and three different fibers were used, and the relevant results were found:

- In the hydration process of White Cement, calcium silicates (C_2S and C_3S) reacted with water, similar to Portland Cement, to form C-S-H gel. While White Cement mortar contained more limestone and white limestone and silicate content in obtaining higher compressive strength values than Ordinary Portland Cement, it also provided a significant advantage in the low amount of Fe_2O_3 and Mn_2O_3, which reduced the pozzolanic activity. In the light of these factors, White Cement has created a stronger matrix structure by increasing the amount of calcium silicate hydrate formed.
- When the brick powder was used up to 5%, it accelerated the pozzolanic reaction and increased the flexural and compressive strength results. In this case, the brick powder had a higher Al_2O_3 and SiO_2 content, accelerating the reaction with CH, and as a result, more C-A-S-H and C-S-H gels were produced that bonded the hydration products. It was also effective in that it created a more refined pore network by acting as a filler. In the case of using higher ratios, a significant decrease in cement content caused a decrease in hydration products such as CH and C-S-H gels, resulting in a decrease in strength.
- Flexural and compressive strength results increased with the effect of fibers. The lower rate of increase in compressive strength was due to the low use of fibers and the main task of the fibers was to resist the cracking effect caused by tensile stress in the lower regions of the samples. Among the fibers, crimped steel fibers made the most important contribution. This was because crimped steel fibers were longer and had a higher density. Thus, by reducing the number of voids, lateral deformations were reduced, thereby increasing the strength. The fact that the crystal phases in basalt fibers had a fine and homogeneous structure and produced a natural nucleator has ensured these fibers showed a systematic performance. Copper-coated steel fiber formed the lowest strength value due to its shortness. In the case of using crimped steel fiber with 5% brick dust, the compressive strength increased by 13% while the flexural strength increased by 21%.
- Significant decreases in the mechanical properties of the samples occurred after high temperature, freeze–thaw, and sulfate effect. The use of 5% brick powder increased the formation of calcium silicate hydrate and increased the performance after durability tests. Similarly, the fibers have braked the strength losses due to the resistance they have created against cracks. Although the decreases caused

Fig. 20. Visual inspection after sulfate effect: a) WC, b) CBP5, c) CBP10, d) CBP15, e) CBP5B, f)WCB, g) WCCC, h) CBP5CC, i)WCC, j)CBP5C.

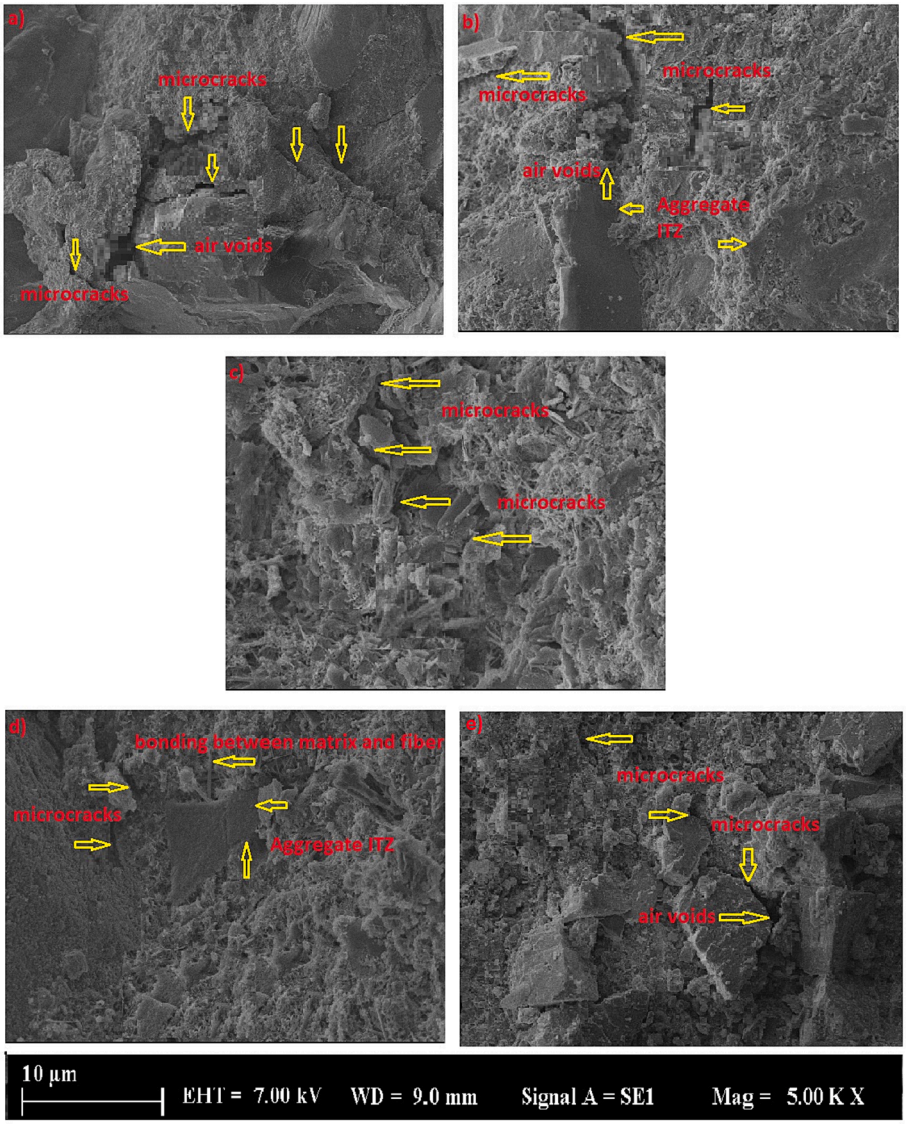

Fig. 21. SEM images of samples after sulfate attack: a) WC, b) CBP5, c) CBP5C, d) CBP5B, and e) CBP5CC.

losses, it was observed that the stability of the samples was preserved. Obtained results were supported by SEM and XRD results.

Declaration of Competing Interest

The authors declare that they have no known competing financial interests or personal relationships that could have appeared to influence the work reported in this paper.

Data availability

No data was used for the research described in the article.

Acknowledgment

We would like to thank Istanbul Gelişim University and Yıldız Technical University for their support during our studies.

References

[1] E. Batuecas, I. Ramón-Álvarez, S. Sánchez-Delgado, M. Torres-Carrasco, Carbon footprint and water use of alkali-activated and hybrid cement mortars, J. Clean. Prod. 319 (2021), 128653.
[2] S. Shagñay, L. Ramón, M. Fernández-Álvarez, A. Bautista, F. Velasco, M. Torres-Carrasco, Eco-efficient hybrid cements: Pozzolanic, mechanical and abrasion properties, Appl. Sci. 10 (24) (2020) 8986.
[3] Yun-Hsun Huang, Wu Jung-Hua, Bottom-up analysis of energy efficiency improvement and CO2 emission reduction potentials in the cement industry for energy transition: An application of extended marginal abatement cost curves, J. Clean. Prod. 296 (2021), 126619.
[4] A. Petit, G. Cordoba, C.I. Paulo, E.F. Irassar, Novel air classification process to sustainable production of manufactured sands for aggregate industry, J. Cleaner Prod. 198 (2018) 112–120.
[5] J. Couvidat, C. Diliberto, E. Meux, S. Cotelle, C. Bojic, L. Izoret, A. Lecomte, Greening effect of slag cement-based concrete: Environmental and ecotoxicological impact, Environ. Technol. Innovation 22 (2021), 101467.
[6] Y. Zhao, M. Yu, Y. Xiang, F. Kong, L. Li, A sustainability comparison between green concretes and traditional concrete using an emergy ternary diagram, J. Cleaner Prod. 256 (2020), 120421.
[7] H. Alabduljabbar, H. Mohammadhosseini, M.M. Tahir, R. Alyousef, Green and sustainable concrete production using carpet fibers waste and palm oil fuel ash, Mater. Today:. Proc. 39 (2021) 929–934.
[8] M. Karimaei, F. Dabbaghi, A. Sadeghi-Nik, M. Dehestani, Mechanical performance of green concrete produced with untreated coal waste aggregates, Constr. Build. Mater. 233 (2020), 117264.
[9] M. Hasanzadeh, O. Rezaifar, M. Gholhaki, M. Kazem Sharbatdar, Performance optimization of ground rubberized green concrete with metakaolin, Structures 34 (2021) 433–448.
[10] A. Ginting, D.H. Pradikta, B. Santosa, P. Adi, Comparison of Compressive Strength of Concrete Using White Portland Cement with Gray Cement, Jurnal Teknik Sipil dan Perencanaan 24 (1) (2022) 1–7.

[11] R. Yang, M. Zhang, Z. Li, F. He, Microstructural insight into the deterioration mechanism of the mortar subject to the combined action of external sulfate attack and cyclic wetting–drying, Constr. Build. Mater. 317 (2022), 125484.
[12] A. Zhang, Y. Ge, W. Yang, X. Cai, Y. Du, Comparative study on the effects of nano-SiO2, nano-Fe2O3 and nano-NiO on hydration and microscopic properties of white cement, Constr. Build. Mater. 228 (2019), 116767.
[13] A. Joshaghani, Evaluating the effects titanium dioxide on resistance of cement mortar against combined chloride and sulfate attack, Struct. Concr. 19 (5) (2018) 1318–1327.
[14] Q. Huang, X. Zhu, G. Xiong, C. Wang, D. Liu, L. Zhao, Recycling of crushed waste clay brick as aggregates in cement mortars: An approach from macro-and micro-scale investigation, Constr. Build. Mater. 274 (2021), 122068.
[15] N.N. Lam, Heat resistant mortar using Portland cement and waste clay bricks, in: CIGOS 2019, Innovation for Sustainable Infrastructure, Springer, Singapore, 2020, pp. 549–554.
[16] J. Shao, J. Gao, Y. Zhao, X. Chen, Study on the pozzolanic reaction of clay brick powder in blended cement pastes, Constr. Build. Mater. 213 (2019) 209–215.
[17] S. Zhang, P. He, L. Niu, Mechanical properties and permeability of fiber-reinforced concrete with recycled aggregate made from waste clay brick, J. Clean. Prod. 268 (2020).
[18] H. Dilbas, Ö. Çakır, Influence of basalt fiber on physical and mechanical properties of treated recycled aggregate concrete, Constr. Build. Mater. 254 (2020).
[19] B. Ali, R. Kurda, B. Herki, R. Alyousef, R. Mustafa, A. Mohammed, A. Raza, H. Ahmed, M. Fayyaz Ul-Haq, Effect of varying steel fiber content on strength and permeability characteristics of high strength concrete with micro silica, Materials 13 (24) (2020) 5739.
[20] A. Celik, K. Yilmaz, O. Canpolat, M.M. Al-mashhadani, Y. Aygörmez, M. Uysal, High-temperature behavior and mechanical characteristics of boron waste additive metakaolin based geopolymer composites reinforced with synthetic fibers, Constr. Build. Mater. 187 (2018) 1190–1203.
[21] Y. Aygörmez, O. Canpolat, M.M. Al-mashhadani, M. Uysal, Elevated temperature, freezing-thawing and wetting-drying effects on polypropylene fiber reinforced metakaolin based geopolymer composites, Constr. Build. Mater. 235 (2020), 117502.
[22] Y. Aygörmez, O. Canpolat, Long-term sulfuric and hydrochloric acid resistance of silica fume and colemanite waste reinforced metakaolin-based geopolymers, Revista de la construcción 20 (2) (2021) 291–307.
[23] I.M. El-Kattan, M.A. Abdelzaher, A.A. Farghali, Positive impact of ultra fine-ceramic waste on the physico-mechanical features and microstructure of white cement pastes composites, J. Mater. Res. Technol. 9 (4) (2020) 9395–9402.
[24] Y. Aygörmez, O. Canpolat, M.M. Al-mashhadani, High-temperature effects on white cement-based slurry infiltrated fiber concrete with metakaolin and fly ash additive, Revista de la construcción 19 (2) (2020) 324–333.
[25] F.S. Klak, A.I. Abdulla, Compressive strength of cement mortar with white cement and limestone, International Journal of, Eng. Technol. 7 (4.37) (2018) 48–52.
[26] P. Rovnaník, P. Rovnanikova, M. Vyšvařil, S. Grzeszczyk, E. Janowska-Renkas, Rheological properties and microstructure of binary waste red brick powder/metakaolin geopolymer, Constr. Build. Mater. 188 (2018) 924–933.
[27] J.M. Ortega, V. Letelier, C. Solas, G. Moriconi, M.Á. Climent, I. Sánchez, Long-term effects of waste brick powder addition in the microstructure and service properties of mortars, Constr. Build. Mater. 182 (2018) 691–702.
[28] Z. Ma, Q. Tang, H. Wu, J. Xu, C. Liang, Mechanical properties and water absorption of cement composites with various fineness and contents of waste brick powder from C&D waste, Cem. Concr. Compos. 114 (2020), 103758.
[29] O.M. Olofinnade, A.N. Ede, C.A. Booth, Sustainability of waste glass powder and clay brick powder as cement substitute in green concrete, Handbook, Environ. Mater. Manag. (2019) 2927–2948.
[30] P. Mahakavi, R. Chithra, Impact resistance, microstructures and digital image processing on self-compacting concrete with hooked end and crimped steel fiber, Constr. Build. Mater. 220 (2019) 651–666.
[31] A. Jalal, N. Shafiq, M. Zahid, Investigating the effects of fiber reinforced concrete on the performance of end-zone of pre-stressed beams, Materials 12 (13) (2019) 2093.
[32] S.J.S. Chelladurai, R. Arthanari, N. Nithyanandam, K. Rajendran, K. K. Radhakrishnan, Investigation of mechanical properties and dry sliding wear behaviour of squeeze cast LM6 aluminium alloy reinforced with copper coated short steel fibers, Trans. Indian Inst. Met. 71 (4) (2018) 813–822.
[33] D. Wang, Y. Ju, H. Shen, L. Xu, Mechanical properties of high performance concrete reinforced with basalt fiber and polypropylene fiber, Constr. Build. Mater. 197 (2019) 464–473.
[34] H. Zhou, B. Jia, H. Huang, Y. Mou, Experimental study on basic mechanical properties of basalt fiber reinforced concrete, Materials 13 (6) (2020) 1362.
[35] K. Ebrahimi, M.J. Daiezadeh, M. Zakertabrizi, F. Zahmatkesh, A.H. Korayem, A review of the impact of micro-and nanoparticles on freeze-thaw durability of hardened concrete: Mechanism perspective, Constr. Build. Mater. 186 (2018) 1105–1113.
[36] D. Zou, Z. Wang, M. Shen, T. Liu, A. Zhou, Improvement in freeze-thaw durability of recycled aggregate permeable concrete with silane modification, Constr. Build. Mater. 268 (2021), 121097.
[37] R. Wang, Z. Hu, Y. Li, K. Wang, H. Zhang, Review on the deterioration and approaches to enhance the durability of concrete in the freeze–thaw environment, Constr. Build. Mater. 321 (2022), 126371.
[38] I.B. Topcu, O. Atesin, T. Uygunoglu, Effect of High Dosage Air-Entraining Admixture Usage on Micro Concrete Properties, Eur. J. Eng. Nat. Sci. (EJENS) 2 (1) (2017) 1–11.
[39] Y. Aygörmez, Evaluation of the red mud and quartz sand on reinforced metazeolite-based geopolymer composites, J. Build. Eng. 43 (2021), 102528.
[40] Y. Aygörmez, O. Canpolat, M.M. Al-mashhadani, Assessment of geopolymer composites durability at one year age, J. Build. Eng. (2020), 101453.
[41] N. Ali, O. Canpolat, Y. Aygörmez, M.M. Al-Mashhadani, Evaluation of the 12–24 mm basalt fibers and boron waste on reinforced metakaolin-based geopolymer, Constr. Build. Mater. 251 (2020), 118976.
[42] Y. Aygörmez, Assessment of performance of metabentonite and metazeolite-based geopolymers with fly ash sand replacement, Constr. Build. Mater. 302 (2021), 124423.
[43] A.A. Arslan, M. Uysal, A. Yılmaz, M.M. Al-mashhadani, O. Canpolat, F. Şahin, Y. Aygörmez, Influence of wetting-drying curing system on the performance of fiber reinforced metakaolin-based geopolymer composites, Constr. Build. Mater. 225 (2019) 909–926.
[44] X. Jiang, R. Xiao, M. Zhang, W. Hu, Y. Bai, B. Huang, A laboratory investigation of steel to fly ash-based geopolymer paste bonding behavior after exposure to elevated temperatures, Constr. Build. Mater. 254 (2020), 119267.
[45] A. Abolhasani, M. Shakouri, M. Dehestani, B. Samali, S. Banihashemi, A comprehensive evaluation of fracture toughness, fracture energy, flexural strength and microstructure of calcium aluminate cement concrete exposed to high temperatures, Eng. Fract. Mech. 261 (2022), 108221.
[46] X. Jiang, Y. Zhang, R. Xiao, P. Polaczyk, M. Zhang, W. Hu, Y. Bai, B. Huang, A comparative study on geopolymers synthesized by different classes of fly ash after exposure to elevated temperatures, J. Cleaner Prod. 270 (2020), 122500.
[47] A.K. Saha, P.K. Sarker, V. Golovanevskiy, Thermal properties and residual strength after high temperature exposure of cement mortar using ferronickel slag aggregate, Constr. Build. Mater. 199 (2019) 601–612.
[48] J.C. Kuri, S. Majhi, P.K. Sarker, A. Mukherjee, Microstructural and non-destructive investigation of the effect of high temperature exposure on ground ferronickel slag blended fly ash geopolymer mortars, J. Build. Eng. 43 (2021), 103099.
[49] F. Althoey, A.K.A. El-Aal, H. Shoukry, I. Hakeem, Performance of Cement Mortars Containing Clay Exposed to High Temperature, Arab. J. Sci. Eng. 47 (1) (2022) 591–599.
[50] B. Li, B. Huo, R. Cao, S. Wang, Y. Zhang, Sulfate resistance of steam cured ferronickel slag blended cement mortar, Cem. Concr. Compos. 96 (2019) 204–211.
[51] H.E. Elyamany, M. Abd Elmoaty, A.M. Elshaboury, Magnesium sulfate resistance of geopolymer mortar, Constr. Build. Mater. 184 (2018) 111–127.
[52] Q. Huang, X. Zhu, L. Zhao, M. Zhao, Y. Liu, X. Zeng, Effect of nanosilica on sulfate resistance of cement mortar under partial immersion, Constr. Build. Mater. 231 (2020), 117180.
[53] M.N. Aziez, A. Bezzar, Effect of temperature and type of sand on the magnesium sulphate attack in sulphate resisting Portland cement mortars, J. Adhes. Sci. Technol. 32 (3) (2018) 272–290.